Suitably impressive thesis title

Mikkel Bjørn
St. Anne's College
University of Oxford

A thesis submitted for the degree of
Doctor of Philosophy
Trinity 2020

Acknowledgements

suitable thank you's

Abstract

World's best measurement of γ. Details to be added.

Contents

Preface

The work presented in this thesis has been resulted in two papers, either under review or published in the Journal of High Energy Physics. These are

> [**?**] *Measurement of the CKM angle γ using $B^\pm \to [K^0_S h^+ h^-]_D h^\pm$ decays*, submitted to JHEP.
> This paper describes a measurement of the CKM angle γ using pp collision data taken with the LHCb experiment during the Run 1 of the LHC, in 2011 and 2012, and during the full Run 2, in 2015–2018. The measurement uses the decay channels $B^\pm \to Dh^\pm$ where $D \to K^0_S h'^+ h'^-$, in which h and h' denotes pions or kaons. It obtains a value of $\gamma = (?\pm?)^\circ$, which constitutes the world's best single-measurement determination of γ. The work is the main focus of this thesis and described in detail in Chapter 4.

> [**?**] *CP violation and material interaction of neutral kaons in measurements of the CKM angle γ using $B^\pm \to DK^\pm$ decays where $D \to K^0_S \pi^+ \pi^-$*, JHEP 19 (2020) 106.
> This paper describes a phenomenological study of the impact of neutral kaon CP violation and material interaction on measurements of γ. With the increased measurement precision to come in the near future, an understanding of these effects is crucial, especially in the context of $B \to D\pi$ decays; however no detailed study had been published at the start of this thesis. The study is the subject of Chapter 3. Some text excerpts and figures from the paper have been reproduced in the thesis.

All of the work described in this thesis is my own, except where clearly referenced to others. Furthermore, I contributed significantly to an analysis of $B^\pm \to DK^\pm$ decays with LHCb data taken in 2015 and 2016, now published in

> [**?**] *Measurement of the CKM angle γ using $B^\pm \to DK^\pm$ with $D \to K^0_S \pi^+ \pi^-$ $K^0_S K^+ K^-$ decays*, JHEP 08 (2018) 176.

I was responsible for the analysis of the signal channel, whereas the control channel was analysed by Nathan Jurik. The measurement is superseded by that of Ref. [**?**] and is not described in detail in the thesis.

1

Theoretical background

This chapter lays out the theoretical framework of the thesis. Section 1.1 introduces charge and parity symmetry violation in general, while Section 1.2 covers the description in the Standard Model and the general theory behind charge-parity symmetry violation measurements in charged B decays. Section 1.3 focuses on the theory of measurements using $B^{\pm} \to Dh^{\pm}$ decays with multi-body D final states, after which the specific analysis strategy for the measurement described in the thesis is outlined out in Section 1.4.

1.1 The C, P and T symmetries and their violation

The concept of symmetry play a fundamental role in modern physics. By Noether's theorem [**?**], the simple assumption of invariance of our physical laws under universal temporal and spatial translations leads to the very non-trivial prediction of conserved energy and momentum; within the field of particle physics, the interactions and dynamics of the Standard Model (SM) follow completely simply from requiring the fundamental particle fields to satisfy a local $U(1) \times SU(2) \times SU(3)$ gauge symmetry [**?**]; and one of the short-comings of the SM, is that it fails to explain the apparent *lack* of symmetry in our matter-dominated universe [**?**]. Indeed, it is important to experimentally establish the symmetries of our world at a fundamental level, and the degree to which they are broken.

I'll adjust this paragraph when I've written the introduction.

Three discrete symmetries of importance are the symmetries under

1. The charge operator C, which conjugates all internal quantum numbers of a quantum state and thus converts particles into their anti-particle counter parts. For example, C transforms the electric charge of a particle state $Q \to -Q$.

2. The parity operator P, which inverts the spatial dimensions of space time: $\vec{x} \to -\vec{x}$. As such, it transforms left-handed particle fields into right-handed particle fields and vice versa.

3. The time-inversion operator T, which inverts the temporal dimension of space time: $t \to -t$.

These are fundamentally related by the CPT theorem [?] , which states that any Lorentz-invariant Quantum Field Theory (QFT) must be symmetric under the simultaneous application of *all* three operators. However, any one of the symmetries can be broken individually, and experiments have shown the physical laws of our world to violate each of the C, P, and T symmetries.

Such a symmetry-breaking effect was established for the first time in 1956, when Chien-Shiung Wu observed parity violation in weak decays of Co-60 nuclei [?], after carrying out an experiment that was proposed by Yang Chen-Ning and Tsung-Dao Lee [?]. While this experiment established the breaking of P symmetry, it left open the possibility that the physical laws are invariant under a combination of a charge- and parity inversion; that they are CP symmetric. However, this was disproved in 1964 when Kronin and Fitch observed that long-lived kaons, which predominantly decay to the CP-odd 3π state, could also decay to the CP-even $\pi\pi$ states [?].

Since then CP violation has been found in the B^0 system by the BaBar and Belle collaborations [?,?] during the early 2000's; the B factories, along with CDF, also saw evidence for CP violation in $B^\pm$ decays [?, ?, ?, ?, ?, ?] later confirmed by LHCb [?], and CP violation was measured for the B_s^0 meson by LHCb in 2013 [?]; within the last year and a half, the first observation of CP-violation in D^0 decays has also been made by the LHCb collaboration [?], and most recently evidence for CP-violation in the neutrino sector has been reported by the T2K collaboration [?]. The observed effects can be divided into distinct classes. The conceptually simplest case is

1. *CP-violation in decay*, where $|A/\bar{A}| \neq 1$ for some decay amplitude A, and the amplitude $\bar{A}$ of the CP-conjugate decay. The result is different decay rates in two CP-conjugate decays

$$\Gamma(M \to f) \neq \Gamma(\bar{M} \to \bar{f}). \tag{1.1}$$

This type of CP violation was not seen until the late 1980ies [?, ?], more than 20 years after the first observation of CP violation, and only finally established around the year 2000 [?, ?]. Also this discovery was made in $K \to \pi\pi$ decays.

CP-violation in decay is the only type possible for charged initial states, and it is thus the main focus of the thesis. Two additional *CP*-violating effect are possible for neutral initial states (a situation that will be the main focus of Chapter 3). These effects are

2. *CP-violation in mixing*, which denotes the case where the mixing rates between the M^0 and $\bar{M}^0$ states differ

$$\Gamma(M^0 \to \bar{M}^0) \neq \Gamma(\bar{M}^0 \to M^0). \tag{1.2}$$

   The *CP* violation first observed by Kronin and Fitch in the neutral kaon sector [**?**] is (dominantly) of this type.

3. *CP-violation in interference between mixing and decay*, which can be present for a neutral initial states M^0 decaying into a final state f common to both M^0 and $\bar{M}^0$. The decay rate includes an interference term between two amplitudes: the amplitude for a direct $M^0 \to f$ decay and the amplitude for a decay after mixing: $M^0 \to \bar{M}^0 \to f$. Even in the absence of the two aforementioned effects, the rates $\Gamma(M^0 \to f)$ and $\Gamma(\bar{M}^0 \to \bar{f})$ can differ due to the interference term. Such *CP* asymmetries have been measured in eg. $B^0 \to J/\psi K$ by LHCb and the B factories, and in $B_s^0 \to J/\psi\phi$ decays by the LHC and Tevatron experiments [**?**].

CP violation measurements thus have a long, rich, and still-developing history.

1.2 CP violation in the Standard Model

All existing measurements of *CP* violation in the quark sector are naturally explained in the SM; indeed, the need to explain the observation *CP* violation in neutral kaons was a driving force in the development of the model in the first place, when it lead Kobayashi and Maskawa to predict the existence of then-unknown particles in 1973 [**?**] (now known to be the third generation quarks).

1.2.1 The CKM matrix and the Unitarity Triangle

The SM contains three generations of quarks, each consisting of an up-type quark (u, c, and t) and a down-type quark (d, s, and b). The charged weak interaction of the $W^{\pm}$ boson couples up and down-type quarks. The quark states that couple to the W are not (a priori) identical to the mass eigenstates, and can be denoted (u', c', and t') and (d', s', and b'). A basis for the quark states can be chosen such that the weakly

coupling up-quark states are identical to the propagating quark states, $u = u'$, but then the down-type quark stare are different: $d' \neq d$. The two bases of the down-type quarks are related via the Cabibbo-Kobayashi-Maskawa (CKM) matrix [?, ?][1]

$$\begin{pmatrix} d' \\ s' \\ t' \end{pmatrix} = V \begin{pmatrix} d \\ s \\ t \end{pmatrix} = \begin{pmatrix} V_{ud} & V_{us} & V_{ub} \\ V_{cd} & V_{cs} & V_{cb} \\ V_{td} & V_{ts} & V_{tb} \end{pmatrix} \begin{pmatrix} d \\ s \\ t \end{pmatrix}. \tag{1.3}$$

Thus the Lagrangian terms representing the coupling of a $W^{\pm}$ boson with a u- and a d-type quark is

$$\mathcal{L}_{W^+} = -\frac{g}{\sqrt{2}} V_{ud} \left(\bar{u} \gamma^{\mu} W^{+}_{\mu} d \right) \qquad \mathcal{L}_{W^-} = -\frac{g}{\sqrt{2}} V^{*}_{ud} \left(\bar{d} \gamma^{\mu} W^{-}_{\mu} u \right) \tag{1.4}$$

where g is the weak coupling constant, γ_u are the Dirac matrices, and u and d represent the left-handed components of the physical quark states.

The CKM matrix is a unitary complex 3×3 matrix, and hence has $3^2 = 9$ independent, real parameters. However, 5 of these can be absorbed into non-physical phases of the quark states (both mass and weak eigenstates) and hence the matrix has 4 real, physical parameters: 3 mixing angles and a single phase. Chau and Keung [?] proposed the parameterisation

$$\begin{aligned} V &= \begin{pmatrix} 1 & 0 & 0 \\ 0 & c_{23} & s_{23} \\ 0 & -s_{23} & c_{23} \end{pmatrix} \begin{pmatrix} c_{13} & 0 & s_{13} e^{-i\delta_{CP}} \\ 0 & 1 & 0 \\ -s_{13} e^{-i\delta_{CP}} & 0 & c_{13} \end{pmatrix} \begin{pmatrix} c_{12} & s_{12} & 0 \\ -s_{12} & c_{12} & 1 \\ 0 & 0 & 1 \end{pmatrix} \\ &= \begin{pmatrix} c_{12} c_{13} & s_{12} c_{13} & s_{13} e^{-i\delta_{CP}} \\ -s_{12} c_{23} - c_{12} s_{23} s_{13} e^{i\delta_{CP}} & c_{12} c_{23} - s_{12} s_{23} s_{13} e^{i\delta_{CP}} & s_{23} c_{13} \\ s_{12} s_{23} - c_{12} c_{23} s_{13} e^{i\delta_{CP}} & -c_{12} s_{23} - s_{12} c_{23} s_{13} e^{i\delta_{CP}} & c_{23} c_{13} \end{pmatrix} \end{aligned} \tag{1.5}$$

which is the preferred standard by the PDG [?]. Here, $s_{ij} \equiv \sin\theta_{ij}$ and $c_{ij} \equiv \cos\theta_{ij}$ denote the sine and cosine of three rotation angles in quark space; $\theta_{12} = \theta_C$ being the usual Cabibbo angle [?].

The presence of the complex phase δ_{CP} in the Lagrangian term of the W coupling causes *CP* violation because, as evident from Eq. (1.4), if δ_{CP} enters the amplitude for some decay mediated by a W boson, $A = |A| e^{i(\delta_0 + \delta_{CP})}$, then it will enter the *CP* conjugate decay amplitude with the opposite sign: $\bar{A} = |A| e^{i(\delta_0 - \delta_{CP})}$. In these expressions, δ_0 denotes a *CP* conserving phase that is not caused by complex terms in the Lagrangian, but arises due to potential intermediate states in the decay

[1] A basis for the quarks can of course be chosen, such that neither the up-quarks or the down-quarks are expressed in their mass eigenstates. In that case the CKM matrix is recovered as $V = U^{*}_{u} U_d$, where $U_{u/d}$ is the unitary transformation matrices that brings the u/d quarks into their mass eigenstates.

amplitude.[2] Usually the underlying mechanism is due to QCD effects, and these *CP* conserving phases are therefore generally dubbed *strong* phases, as opposed to the *CP* violating *weak* phase of the W coupling [**?**]. This terminology will be applied throughout the thesis.

Experimentally, it has been observed that the CKM matrix elements of Eq. (1.5) satisfy $s_{13} \ll s_{23} \ll s_{12}$. This motivates an often used, alternative parameterisation of the matrix, where the elements are expressed as power series in a parameter λ that naturally incorporates this hierarchy: the Wolfenstein parameterisation [**?**]. The definitions

$$\begin{aligned} s_{12} &\equiv \lambda \\ s_{23} &\equiv \lambda^2 A \\ s_{13} &\equiv \lambda^3(\rho - i\eta) \end{aligned} \tag{1.6}$$

are made, after which the unitarity conditions (or Eq. 1.5) determine the remaining elements to any order in λ.[3] To $\mathcal{O}(\lambda^5)$ the Wolfenstein parameterisation of the CKM matrix is [**?**, **?**]

$$V = \begin{pmatrix} 1 - \frac{\lambda^2}{2} - \frac{\lambda^4}{8} & \lambda & A\lambda^3(\rho - i\eta) \\ -\lambda + \frac{\lambda^5}{2}A^2(1 - 2(\rho + i\eta)) & 1 - \frac{\lambda^2}{2} - \frac{\lambda^4}{8}(1 + 4A^2) & A\lambda^2 \\ A\lambda^3(1 - (\rho + i\eta)(1 - \frac{\lambda^2}{2})) & -A\lambda^2(1 - \frac{\lambda^2}{2}(1 - 2(\rho + i\eta))) & 1 - \frac{1}{2}A^2\lambda^4 \end{pmatrix}. \tag{1.7}$$

The unitarity condition $V^\dagger V = \mathbb{1}$ of the CKM matrix defines 9 relations between the CKM elements of the form

$$\sum_j V_{jq}^* V_{jq} = 1 \quad , \quad q \in \{d, s, b\} \qquad \text{along the diagonal} \tag{1.8a}$$

$$\sum_j V_{jq}^* V_{jq'} = 0 \quad , \quad q, q' \in \{d, s, b\}, q \neq q' \qquad \text{off-diagonal.} \tag{1.8b}$$

The off-diagonal conditions constrain three complex numbers to sum to zero, and can thus be visualised as triangles in the complex plane, the so-called unitarity triangles. Of these, the triangle corresponding to the (d, b) elements plays a special role, because all three sides are of the same order of magnitude, $\mathcal{O}(\lambda^3)$. When expressed in the form

$$\frac{V_{ud}^* V_{ub}}{V_{cd}^* V_{cb}} + \frac{V_{td}^* V_{tb}}{V_{cd}^* V_{cb}} + 1 = 0, \tag{1.9}$$

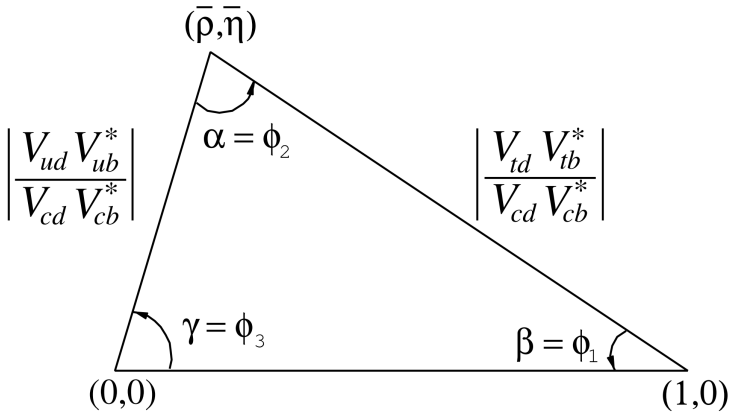

Figure 1.1: Definition of the lengths and sides of the Unitarity Triangle. Figure is taken from the *CKM Quark-Mixing Matrix* review of the PDG [?].

it is often referred to as the singular Unitarity Triangle, illustrated in Fig. 1.1 where the usual names for the three angles are also given.

Over-constraining the unitarity triangle by making separate measurements of all sides and angles, in as many different decay channels as possible, is an important, and non-trivial test of the SM. The current experimental constraints are in agreement with the SM predictions, as visualised in Fig. 1.2. The CKM angle

$$\gamma \equiv \arg(-V_{ud}V_{ub}^*/V_{cd}V_{cb}^*) = \arg(-V_{cb}V_{cd}^*/V_{ub}V_{ud}^*) \tag{1.10}$$

is unique among the CKM parameters, in that it can be measured in tree-level processes without significant theoretical uncertainty from lattice QCD calculations [?]. Because tree-level processes are less likely to be affected by Beyond-Standard-Model (BSM) effects, direct measurements of γ can be considered a SM benchmark, which can be compared to estimates based on measurements of other CKM elements that are measured in loop-level processes, and thus are more likely to be affected by BSM effects [?]. The current, worldwide combination of direct measurements, published by the CKMFitter group, is $\gamma = (72.1^{+5.4}_{-5.7})^\circ$, to be compared with the estimate from loop-level observables of $\gamma = (65.66^{+0.90}_{-2.65})^\circ$ [?]. Other world averages exist [?, ?], but the overall picture is the same: the ability to constrain BSM physics is currently limited by the uncertainty of the direct measurements. Hence further precision measurements of γ are highly motivated. Presently, the precision is driven by time-integrated measurements of direct *CP*-violation in $B^\pm \to DK^\pm$ decays;

Not sure if I should spend time explaining the non-gamma measurements entering?

[2] It is generally true that all phases of a single term in a given amplitude will be convention dependent, but that the phase differences between terms are not.

[3] Other variants of the Wolfenstein parameterisation do exist [?]. They all agree at the lowest orders of λ.

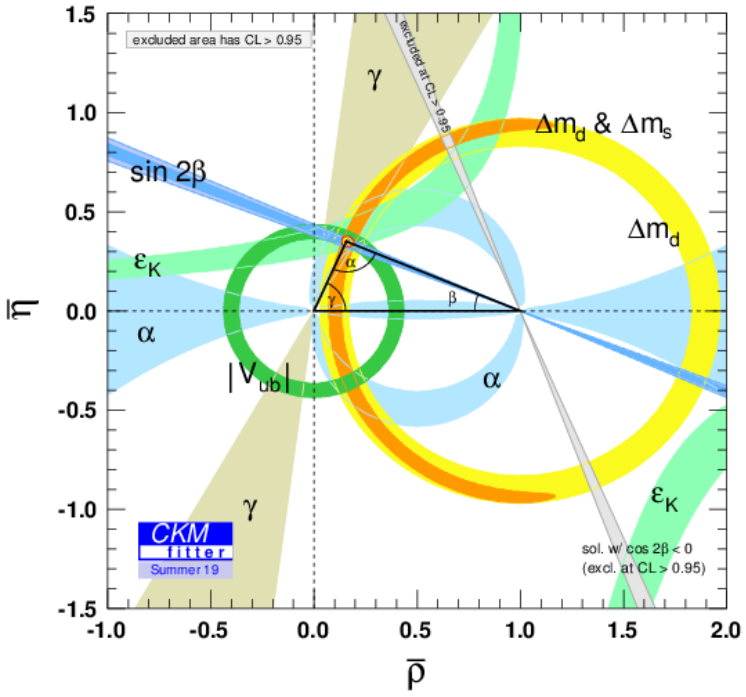

Figure 1.2: Current constraints on the Unitarity Triangle parameters as determined by the CKMFitter group for the EPS 2019 conference [**?**].

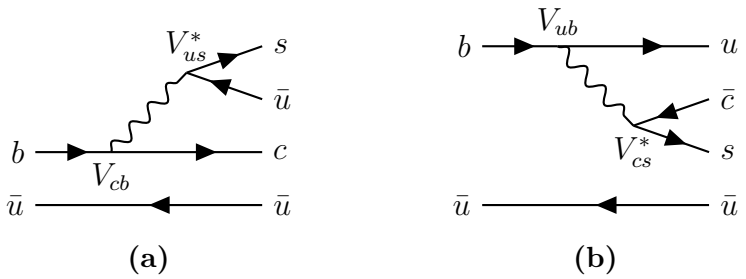

Figure 1.3: Tree level Feynman diagrams describing (a) $B^- \to D^0 K^-$ and (b) $B^- \to \overline{D}^0 K^-$ decays. The electro-weak phase difference between the two decays is $\Delta\phi = \arg\left(V_{cb}V_{us}^*/V_{ub}V_{cs}^*\right) \simeq \gamma$.

such a measurement is the topic of this thesis and the theory behind is treated in detail in the following section. It is also possible to measure γ in time-dependent mixing analyses of $B_s^0 \to D_s^{\mp} K^{\pm}$, $B^0 \to D^{\mp}\pi^{\pm}$ and related decays, by measuring *CP* violation in interference between mixing and decay. These modes are expected to provide competitive measurements in the future [**?**, **?**].

1.2.2 Measuring γ in tree level decays

The phase γ can be measured in tree-level processes with interference between $b \to cs\bar{u}$ and $b \to \bar{c}su$ transitions. The canonical example, also the subject of this thesis, is based on measurements sensitive to interference between the $B^\pm \to D^0 K^\pm$ and $B^\pm \to \overline{D}^0 K^\pm$ decay amplitudes. As illustrated in Fig. 1.3 for the case of B^- decays, the electro-weak phase difference between the two decays is $\Delta\phi = \arg\left(V_{cb}V_{us}^*/V_{ub}V_{cs}^*\right)$. While $\Delta\phi$ is not identical to the definition of γ in Eq. (1.10), the ratio of the involved CKM matrix elements is [**?**]

$$\begin{aligned} -\frac{V_{cd}^*/V_{ud}^*}{V_{us}^*/V_{cs}^*} &= -\frac{-\lambda[1-\frac{\lambda^4}{2}A^2(1-2(\rho-i\eta))](1-\frac{\lambda^2}{2}-\frac{\lambda^4}{8}(1+4A^2))}{\lambda(1-\frac{\lambda^2}{2}-\frac{\lambda^4}{4})} \\ &= 1-\lambda^4A^2(1-2(\rho-i\eta))+\mathcal{O}(\lambda^5). \end{aligned} \tag{1.11}$$

The ratio equals unity to $\mathcal{O}(\lambda^4) \simeq 2.6 \times 10^{-3}$, and thus $\Delta\phi \simeq \gamma$ is a good approximation within current experimental uncertainties. For the remainder of this thesis the approximation will be used without further comment. The diagrams in Fig. 1.3 describe the leading order contributions to the two amplitudes

$$\begin{aligned} A[B^- \to D^0 K^-] &\equiv A_B \\ A[B^- \to \overline{D}^0 K^-] &\equiv \bar{A}_B \equiv r_B A_B e^{i(\delta_B-\gamma)}, \end{aligned} \tag{1.12a}$$

where the last equality introduces two new parameters: the amplitude magnitude ratio $r_B \equiv |\bar{A}_B|/|A_B|$, and δ_B, the strong-phase difference between the decay amplitudes. Since all *CP*-violation is attributed to the electro-weak phase in the SM, the *CP*-conjugate decay amplitudes are [**?**]

$$\begin{aligned} A[B^+ \to \overline{D}^0 K^+] &= A_B \\ A[B^+ \to D^0 K^+] &= \bar{A}_B = r_B A_B e^{i(\delta_B+\gamma)}. \end{aligned} \tag{1.12b}$$

In an experimental setting, the D^0 and $\overline{D}^0$ mesons are reconstructed in some final state, f or its *CP*-conjugate $\bar{f}$. In analogy with the $B^\pm$ decays, the D decay amplitude can be related[4]

$$\begin{aligned} A[D^0 \to f] &= A[\overline{D}^0 \to \bar{f}] = A_D \\ A[\overline{D}^0 \to f] &= A[D^0 \to \bar{f}] = r_D A_D e^{i\delta_D}. \end{aligned} \tag{1.13}$$

where the assumption has been made that *CP* violation in the D decays is negligible, and δ_D denotes a *CP*-conserving strong-phase difference. While *CP*-violation in

[4] In this notation δ_D is thus phase of the suppressed D-decay amplitude minus the phase of the favoured D-decay amplitude. This is the opposite convention to that used in the LHCb measurements with the ADS technique, but aligns with the notation used in the literature on γ measurements in $D \to K^0_S\pi^+\pi^-$ decays.

D decays has recently been measured [**?**], the size of the effect is small and it is considered negligible in this thesis. Based on Eqs. 1.12 and (1.13), the decay rates of B^+ and B^- mesons into the possible final states can be seen to satisfy

$$\Gamma(B^- \to D(\to f)K^-) \propto 1 + r_D^2 r_B^2 + 2r_B r_D \cos\left[\delta_B + \delta_D - \gamma\right], \tag{1.14a}$$
$$\Gamma(B^+ \to D(\to \bar{f})K^+) \propto 1 + r_D^2 r_B^2 + 2r_B r_D \cos\left[\delta_B + \delta_D + \gamma\right], \tag{1.14b}$$
$$\Gamma(B^- \to D(\to \bar{f})K^-) \propto r_D^2 + \ r_B^2 + 2r_B r_D \cos\left[\delta_B - \delta_D - \gamma\right], \tag{1.14c}$$
$$\Gamma(B^+ \to D(\to f)K^+) \propto r_D^2 + \ r_B^2 + 2r_B r_D \cos\left[\delta_B - \delta_D + \gamma\right]. \tag{1.14d}$$

The processes in Eqs. (1.14a) and (1.14b) are *CP*-conjugate and it is clear how, in the general case where $\delta_B + \delta_D \neq 0$, a non-zero value of γ leads to *CP* violation in the form of differing decay rates. The same is true for the processes in Eqs. (1.14c) and (1.14d). Depending on the choice of D final state, these expressions can be used to relate γ to various observables that are experimentally accessible. This thesis concerns the choice $f = K^0_S\pi^+\pi^-$ or $f = K^0_S K^+ K^-$, where the terms related to the D decay all have a non-trivial variation over the phase space of the decay. However, it is useful to first analyse the simpler case where f is a two-body state.

The simplest case is when f is chosen to be a *CP* eigenstate, so that $f = \pm\bar{f}$ and the rate equations of (1.14a)–(1.14d) simplify, because $r_D = 1$ and $\delta_D \in \{0, \pi\}$. Measurements of γ in such decay modes are denoted GLW measurements, after Gronau, London, and Wyler who described the approach in the early 90ies [**?**, **?**]. Experimentally it is preferable to measure yield ratios rather than absolute rates, and the observables of interest are thus the *CP* asymmetry

$$\begin{aligned} A_{CP=\pm1} &= \frac{\Gamma[B^- \to D_{CP}K^-] - \Gamma[B^+ \to D_{CP}K^+]}{\Gamma[B^- \to D_{CP}K^-] + \Gamma[B^+ \to D_{CP}K^+]} \\ &= \frac{\pm r_B \sin\delta_B \sin\gamma}{1 + r_B^2 \pm 2r_B \cos\delta_B \cos\gamma}, \end{aligned} \tag{1.15a}$$

as well as the ratio

$$\begin{aligned} R_{CP=\pm1} &= 2\frac{\Gamma[B^- \to D_{CP}K^-] + \Gamma[B^+ \to D_{CP}K^+]}{\Gamma[B^- \to D^0K^-] + \Gamma[B^+ \to \overline{D}^0K^+]} \\ &= 1 + r_B^2 \pm 2r_B \cos\delta_B \cos\gamma. \end{aligned} \tag{1.15b}$$

In practice, A_{CP} and R_{CP} are obtained from measured yield ratios that are corrected with appropriate branching fractions. A measurement of A_{CP} and R_{CP} alone is not sufficient to determine the underlying physics parameters (γ, r_B, δ_B), and this is not solely due to the number of parameters exceeding the number of constraints: the equations also allow for multiple, ambiguous solutions for (γ, δ_B). One way to break the ambiguity, first noted in the original paper [**?**], is to make further

measurements in additional B decays. These can be described with the formalism described above, but will not share the same ambiguous solutions because (r_B, δ_B) are unique to a given B decay. Another method is to analyse D decay final states that are not *CP* eigenstates.

A few years later, Atwood, Dunietz, and Sonis analysed an alternative choice of D final states: a simultaneous analysis of a Cabibbo-favoured (CF) decay $D^0 \to f$ and the doubly-Cabibbo-suppressed (DCS) decay $D^0 \to \bar{f}$ into the *CP* conjugate final state [**?**, **?**]. Their suggested method is named the ADS method after the authors. The classical example is to take $f = K^-\pi^+$ and $\bar{f} = \pi^-K^+$. The relative suppression means that the r_D of Eq. (1.14) is small, typically of the same order of magnitude as r_B, and thus the *CP* asymmetry of the suppressed decay is $\mathcal{O}(1)$:

$$\begin{aligned} A_{ADS(\bar{f})} &= \frac{\Gamma[B^- \to D(\to \bar{f})K^-] - \Gamma[B^+ \to D(\to f)K^+]}{\Gamma[B^- \to D(\to \bar{f})K^-] + \Gamma[B^+ \to D(\to f)K^+]} \\ &= \frac{r_D r_B \sin(\delta_B - \delta_D)\sin\gamma}{r_D^2 + r_B^2 + 2r_D r_B \cos(\delta_B - \delta_D)\cos\gamma}. \end{aligned} \tag{1.16a}$$

The large *CP* asymmetry is a prime feature of the ADS method. However, also the suppressed-to-favoured yield ratio is sensitive to the physics parameters of interest:

$$\begin{aligned} R_{ADS(\bar{f})} &= \frac{\Gamma[B^- \to D(\to \bar{f})K^-] + \Gamma[B^+ \to D(\to f)K^+]}{\Gamma[B^- \to D(\to f)K^-] + \Gamma[B^+ \to D(\to \bar{f})K^+]} \\ &= \frac{r_B^2 + r_D^2 + 2r_D r_B \cos(\delta_B - \delta_D)\cos\gamma}{1 + r_D^2 r_B^2 + 2r_D r_B \cos(\delta_B + \delta_D)\cos\gamma}. \end{aligned} \tag{1.16b}$$

The interpretation of A_{ADS} and R_{ADS} in terms of (γ, r_B, δ_B) requires knowledge of the r_D and δ_D parameters, but these can be measured independently. In general, the constraints from a single set of ADS observables suffer the same ambiguities as in the GLW case. However, unlike the GLW case, each D decay mode provides an independent set of constraints, because the parameters related to the D decay vary.

The discussion of this section has centred on the classical case of $B^\pm \to DK^\pm$ decays with a two-body D final state. With minor modifications the techniques have been used to make measurements of γ in B^0 decays [**?**], with B decay final states including excited D mesons [**?**], excited kaons [**?**], or pions [**?**]. The decay $B^\pm \to D\pi^\pm$ also is also *CP*-violating, although the effect is much smaller than in the $B^\pm \to DK^\pm$ decay, because it expected that $r_B^{D\pi^\pm} \simeq 0.005$ [**?**], whereas $r_B^{DK^\pm} \simeq 0.1$. Furthermore, it is possible to use multi-body D final states. However, in some cases, a better precision can then be obtained by exploiting phase-space dependent decay rates. This is the topic of the next section.

1.3 Measuring γ using multi-body D final states

In multi-body D decays, the r_D and δ_D parameters of the fundamental rate equations in Eq. (1.14) vary over the phase space of the D decay. This section describes a model-independent approach to measure γ in $B \to D(\to K^0_S\pi^+\pi^-)h^\pm$ decays by exploiting this variation. The theory is identical for $D \to K^0_S K^+K^-$ decays, and similar ideas have been proposed for the $D \to K^0_S\pi^+\pi^-\pi^0$ [**?**] and $D \to 2\pi^+2\pi^-$ modes [**?**]. First, however, the formalism for describing amplitudes of multi-body decays is briefly reviewed.

1.3.1 Dalitz plots and the phase space of multi-body decays

In general, the phase space of the n-body decay $P \to p_1 + p_2 + ... + p_n$ consists of n four momenta, with a total of $4n$ components. The requirement that each of the final state particles is on-shell provides n constraints on these components, and energy-momentum conservation removes a further 4 degrees of freedom. If the original particle P is s *scalar*, the decay is isotropic, which removes an additional 3 degrees of freedom, leaving the total number of degrees of freedom at $3n-7$. For the specific case of three-body decays, the available phase space can thus be parameterised with only two parameters. A practical and often used choice is the invariant masses

$$s_{12} = m^2(p_1p_2) = (p_1^\mu + p_2^\mu)^2, \qquad s_{13} = m^2(p_1p_3) = (p_1^\mu + p_3^\mu)^2. \tag{1.17}$$

The choice of particle pairs is arbitrary, and the coordinates easily related

$$m_P^2 + m_{p_1}^2 + m_{p_2}^2 + m_{p_3}^2 = m^2(p_1p_2) + m^2(p_1p_3) + m^2(p_2p_3). \tag{1.18}$$

A scatter plot of (s_{12}, s_{13}) values for a sample of particle decays is denoted a Dalitz plot [**?**]. It has the very useful feature that the presence of (narrow) resonances in the decay leads to visible bands in the scatter plot. Figure 1.4 illustrates how the limits of the Dalitz plot are defined by kinematic constraints, and shows an example of a Dalitz plot for $D \to K^0_S\pi^+\pi^-$ decays in which the $K^*(892)^\pm$ and $\rho(770)$ resonances are clearly visible. The plot shows the sample of $B^+ \to D\pi^+$ decays used to make the measurement described in Chapter 4 and thus the D meson is in a superposition of D^0 and $\overline{D}^0$ states (as detailed in the following section).

In terms of the coordinates of Eq. (1.17) the differential decay rate is given by

$$\mathrm{d}\Gamma = \frac{1}{32(2\pi)^3 m_P^3}|\mathcal{M}|^2\,\mathrm{d}s_{12}\mathrm{d}s_{13}, \tag{1.19}$$

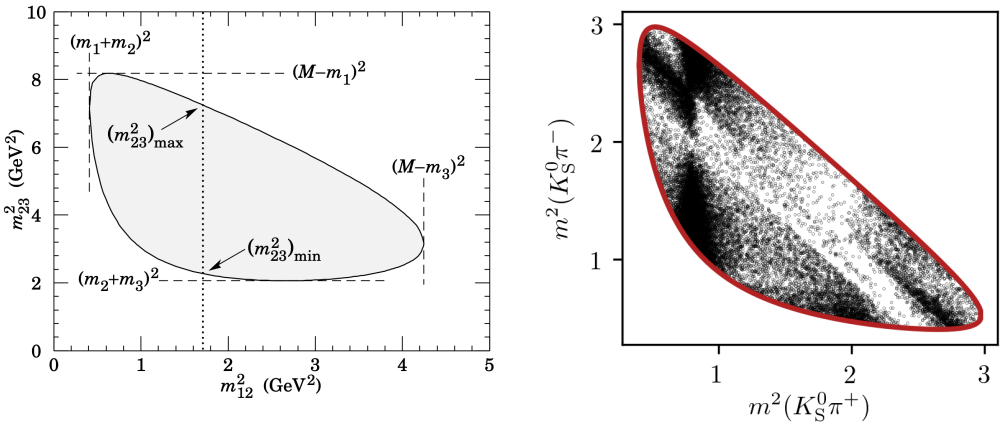

Figure 1.4: (Left) Schematic of a Dalitz plot and the limits of the kinematically allowed phase space limits. (Right) Example of a Dalitz plot for $D \to K^0_S\pi^+\pi^-$ decays where the D meson originates in a $B^+ \to D\pi^+$ decay; the decaying D meson is in a superposition of the D^0 and $\overline{D}^0$ states, but predominantly $\overline{D}^0$-like.

where $\mathcal{M}$ is the QFT matrix element, or total decay amplitude, corresponding to the decay. In general, it is not possible to calculate $\mathcal{M}$ from first principles. Instead, a model is defined with an empirically well motivated form, in which a number of free parameters must be determined experimentally. The simplest case is that of an *isobar* model, where it is assumed that the full decay can be decomposed into consecutive two-body decays of the form $P \to R_{12}(\to p_1 + p_2)p_3$. Thus, $\mathcal{M}$ is expressed as a non-resonant constant amplitude term, k_{NR}, plus a sum of resonance terms

$$\mathcal{M}(s_{12}, s_{13}) = k_{NR} + \sum_r k_r \mathcal{M}^r(s_{12}, s_{13}). \tag{1.20}$$

The exact form of the $\mathcal{M}^r$ function depends on the resonance in question. An overview is given in the PDG review on resonances and references therein [**?**]. The isobar formalism breaks down when resonances in the decay are not well separated. In this case, models of the form in Eq. (3.27) can still be employed, if the contribution from overlapping resonances are collected in a single term. An example of such a model, is the amplitude model for $D^0 \to K^0_S\pi^+\pi^-$ decays developed by the Belle collaboration for a measurement of the CKM angle β in 2018 [**?**]. In this model, individual terms are included for $D^0 \to K^*(\to K^0_S\pi^\pm)\pi^\mp$ decays, whereas the $\pi\pi$ and $K\pi$ S-wave contributions are modelled with the so-called K-matrix- and LASS formalisms [**?**, **?**]. The amplitude and phase of $\mathcal{M}$ as predicted by this model are shown in Fig. 1.5.

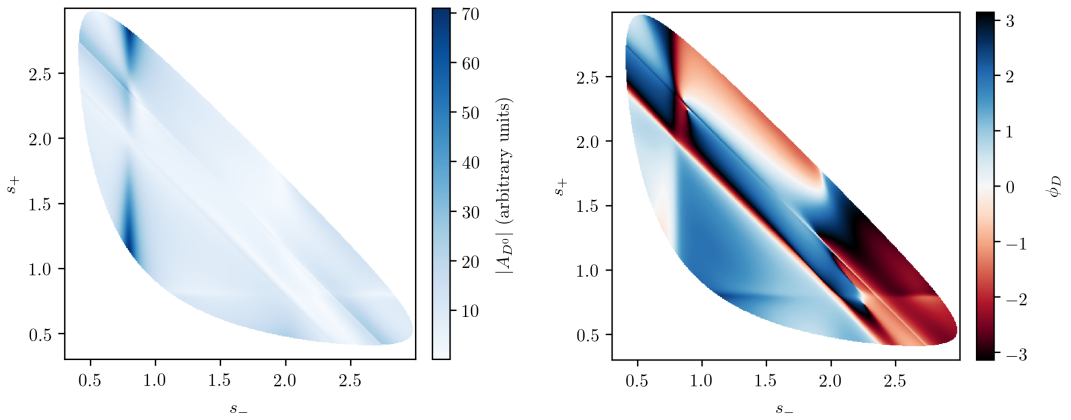

Figure 1.5: The (left) magnitude and (right) phase of the $D \to K^0_S\pi^+\pi^-$ amplitude in the Belle 2018 model [**?**].

1.3.2 The GGSZ method to measure γ

The non-trivial phase-space dependence of the $D \to K^0_S\pi^+\pi^-$ decay amplitude can be exploited to measure γ with $B^\pm \to DK^\pm$ or $B^\pm \to D\pi^\pm$ decays. This approach was proposed independently by Bondar [**?**], and by Giri, Grossman, Soffer, and Zupan [**?**] after whom it takes the commonly used acronym GGSZ. For this specific decay s_- and s_+ are used to described the Dalitz coordinates $m^2(K^0_S\pi^-)$ and $m^2(K^0_S\pi^+)$, respectively, and the D decay amplitude is a function of these coordinates

$$A_S^{(\overline{D})}(s_-, s_+) = A(\overline{(D)}^0 \to K^0_S\pi^+\pi^-). \tag{1.21}$$

To a good approximation the K^0_S meson is a *CP* eigenstate, meaning that the $K^0_S\pi^+\pi^-$ state is self-conjugate. Assuming this approximation to be exact, and that *CP* violation in the D decay is negligible, the D decay amplitude satisfies the symmetry relation

$$A_S^{\overline{D}}(s_-, s_+) = A_S^{D}(s_+, s_-). \tag{1.22}$$

The impact of the K^0_S meson *not* being an exact *CP* eigenstate is treated in detail in Chapter 3. In order to simplify equations, the short-hand notation

$$(s_{-+}) = (s_-, s_+), \qquad (s_{+-}) = (s_+, s_-) \tag{1.23}$$

will be employed for the remainder of the thesis, so that the relation in Eq. (1.22) can be expressed as $A_S^{\overline{D}}(s_{-+}) = A_S^{D}(s_{+-})$. Thus, the rate equations of Eq. (1.14)

for the $D \to K^0_S\pi^+\pi^-$ decay mode are

$$\begin{aligned}
\mathrm{d}\Gamma^-(\mathrm{s}_{-+}) \propto |\mathcal{A}^-_S|^2 &= |A_B|^2|A_{K^0_S}|^2 \\
&\times \Big[|A^D_S(s_{-+})|^2 + r_B^2|A^D_S(s_{+-})|^2 + 2r_B|A^D_S(s_{-+})||A^D_S(s_{+-})| \\
&\times (\cos[\delta_D(s_{-+})]\cos[\delta_B-\gamma] + \sin[\delta_D(s_{-+})]\sin[\delta_B-\gamma])\Big]\,, \quad (1.24a) \\
\mathrm{d}\Gamma^+(\mathrm{s}_{-+}) \propto |\mathcal{A}^+_S|^2 &= |A_B|^2|A_{K^0_S}|^2 \\
&\times \Big[|A^D_S(s_{+-})|^2 + r_B^2|A^D_S(s_{-+})|^2 + 2r_B|A^D_S(s_{-+})||A^D_S(s_{+-})| \\
&\times (\cos[\delta_D(s_{-+})]\cos[\delta_B+\gamma] - \sin[\delta_D(s_{-+})]\sin[\delta_B+\gamma])\Big]\,. \quad (1.24b)
\end{aligned}$$

Here, $\delta_D(s_{-+}) = \phi_D(s_{-+}) - \phi_D(s_{+-}) = -\delta_D(s_{+-})$, where $\phi_D(s_{-+})$ denotes the complex phase of the $A^D_S(s_{-+})$ amplitude, and a standard trigonometric relation have been employed to factorise the terms depending on the complex phases of the B and D decays. It can be seen that in the case where $\gamma = 0$ the B^+ and B^- decay rates are symmetric if the Dalitz coordinates are exchanged: $\Gamma^+(s_-, s_+) = \Gamma^-(s_+, s_-)$. The presence of *CP* violation in the B decay breaks the symmetry. Therefore it is possible to measure γ (and the nuisance parameters r_B and δ_B) from the phase-space distribution of $B^\pm \to D(\to K^0_S\pi^+\pi^-)K^\pm$ decays, given knowledge of $A^D_S(s_{-+})$.

A series of measurements of γ have been made that use amplitude models of the D decay [**?**, **?**, **?**, **?**, **?**, **?**, **?**, **?**]. However, a model-independent approach has been proposed by Bondar and Poluektov [**?**, **?**] that relies on binning phase-space, in which case the necessary information on the D decay amplitude can be summarised in a small set of coefficients that can be measured in a separate experiment. That is the approach followed in this thesis, and has been used previously by the Belle [**?**] and LHCb collaborations [**?**]. It is described in detail in the following section.

Such a model-independent approach is favourable for two reasons. Firstly, uncertainty estimates related to model inputs and the choice of parameterisation in an amplitude model are non-trivial, yet would become the leading systematic with the very high precision expected for γ measurements in the near future. Secondly, amplitude models are notoriously hard to reproduce, and in a high-precision era it is favourable that any experiment is easy to reinterpret in various extensions of the SM. This is a lot easier for an experiment that measures a small set of well-defined observables, than for an experiment that fits a complicated amplitude model.

An alternative model-independent approach has recently been proposed by Poluektov [**?**] where the externally measured input on the D-decay phase are Fourier expansion coefficients, and which therefore avoids binning phase space; this approach may have the potential to improve the obtainable precision in the future.

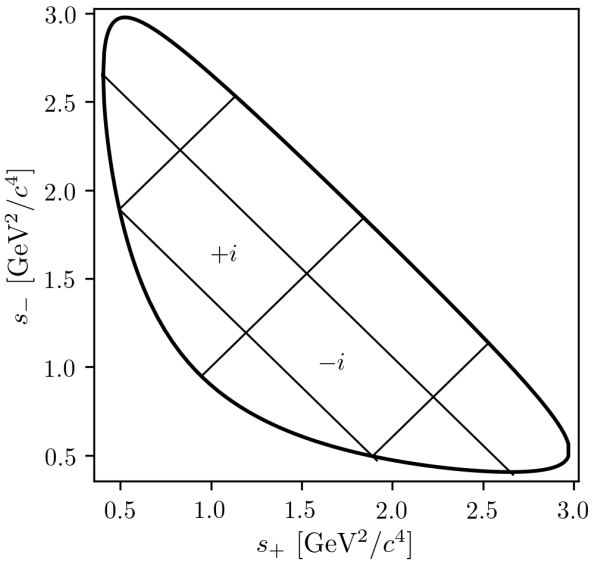

Figure 1.6: Illustration of the binning scheme used in GGSZ measurements: the bins are symmetric around the $m^2(K^0_S\pi^+) = m^2(K^0_S\pi^-$ diagonal, and numbered so that opposite bins have the same number, but with opposite sign.

1.3.3 A model-independent approach

The phase-space distribution can be analysed in a model-independent way, if the D-decay phase space is split into regions, or bins, an the B decay yield in each bin determined experimentally. A measurement of γ using this approach is the main topic of the thesis. This section describes the fundamental principle, whereas the details pertaining to the exact experimental approach are delegated to Section 1.4.

The amplitude symmetry of Eq. (1.22) is exploited by defining $2N$ bins to be symmetric symmetric around the $s_- = s_+$ diagonal of the Dalitz plot, numbered $i = -N$ to N (omitting zero) such that if the point (s_-, s_+) is in bin i, then (s_+, s_-) is in bin $-i$, and by convention $i > 0$ for bins where $s_- > s_+$. The principle is illustrated in Fig. 1.6, but the binning schemes used in actual measurements are more complicated. The decay rates in Eq. (1.24) can be integrated over such bins, and give the bin yields

$$\begin{aligned} N_i^- &\propto h^- \left[K_i + r_B^2 K_{-i} + 2\sqrt{K_i K_{-i}}\,(c_i x_- + s_i y_-) \right], \\ N_i^+ &\propto h^+ \left[K_{-i} + r_B^2 K_i + 2\sqrt{K_i K_{-i}}\,(c_i x_+ - s_i y_+) \right], \end{aligned} \tag{1.25}$$

where the parameters describing the B decay have been expressed in terms of the observables

$$x_\pm = r_B \cos(\delta_B \pm \gamma), \qquad y_\pm = r_B \sin(\delta_B \pm \gamma), \tag{1.26}$$

and a number of phase-space integrated quantities related to the D-decay have been introduced. The K_i parameters denote fractional yield of a flavour-tagged D^0 decaying into bin i, defined as

$$K_i = \frac{1}{N_K}\int_i \mathrm{d}s^2 |A_{\mathrm{S}}^D(s_{-+})|^2, \qquad N_K = \int \mathrm{d}s^2 |A_{\mathrm{S}}^D(s_{-+})|^2, \tag{1.27}$$

where $\int_i \mathrm{d}s^2$ denotes integration over bin i of the Dalitz plot. The c_i and s_i denote the amplitude-weighted average of $\cos\delta_D(s_{-+})$ and $\sin\delta_D(s_{-+})$ over bin i

$$\begin{aligned} c_i &= \frac{\int_i \mathrm{d}s^2 |A_{\mathrm{S}}^D(s_{-+})||A_{\mathrm{S}}^D(s_{+-})|\cos[\delta_D(s_{-+})]}{\sqrt{\int_i \mathrm{d}s^2 |A_{\mathrm{S}}^D(s_{-+})|^2}\sqrt{\int_i \mathrm{d}s^2 |A_{\mathrm{S}}^D(s_{+-})|^2}}, \\ s_i &= \frac{\int_i \mathrm{d}s^2 |A_{\mathrm{S}}^D(s_{-+})||A_{\mathrm{S}}^D(s_{+-})|\sin[\delta_D(s_{-+})]}{\sqrt{\int_i \mathrm{d}s^2 |A_{\mathrm{S}}^D(s_{-+})|^2}\sqrt{\int_i \mathrm{d}s^2 |A_{\mathrm{S}}^D(s_{+-})|^2}}. \end{aligned} \tag{1.28}$$

By the symmetry properties of $\delta_D(s_{-+})$ these parameters satisfy $c_i = c_{-i}$ and $s_i = -s_{-i}$. The normalisation constants h^+ and h^- are identical in the ideal case, but it is convenient to define them separately for practical reasons: depending on the experimental setup, there may be overall production and detection asymmetries that affect the total signal yields. An experimental analysis can be made insensitive to these effects because they can be absorbed into the normalisation constants, as long as they are constant over the D-decay phase space. This comes at the cost that the information on $x_\pm$ and $y_\pm$ from the overall CP asymmetry is lost, but Section 1.3.5 will show the loss in precision to be minimal.

Thus, for a set of $2N$ bins, the bin yields of Eqs. (1.25) provide $4N$ constraints on a total of $4N + 6$ parameters: $(h^\pm, K_i, c_i, s_i, x_\pm, y_\pm)$. However, the K_i, c_i, and s_i parameters relate only to the D decay, and can thus, in principle, be measured in independent experiments. With such external inputs, a measurement of the $B^\pm \to D(\to K^0_{\mathrm{S}}\pi^+\pi^-)K^\pm$ yields in a set of bins can be used to constrain $x_\pm$ and $y_\pm$, and thereby (γ, r_B, δ_B). The measurement presented in this thesis determines the K_i parameters directly, but uses externally measured values of c_i and s_i as input, as measured in quantum correlated D decays by the CLEO [**?**] and BESIII [**?**] collaborations. Because these measurements are the foundation of the approach, they are described in some detail in the following section. In the future, it is possible that the c_i and s_i parameters may be measured in quantum-correlated D decays in LHCb [**?**], and in charm-mixing measurements [**?**].

1.3.4 Measuring strong-phase inputs at charm factories

The strong-phase parameters c_i and s_i have been measured by the CLEO and BESIII collaborations, using quantum correlated $D^0\overline{D}^0$ pairs from decays of the $\psi(3770)$ resonance state, itself produced in e^+e^- collisions at the resonance energy. The $\psi(3770)$ has quantum-number $C = -1$, which is conserved in the strong decay into two D mesons, and thus the two D mesons are produced in an anti-symmetric wave function. By observing the decay of one D meson into a specific final state, say a *CP* eigenstate, the quantum state of the other D meson can be determined. The measurement is based on decays where both D decays are reconstructed, one in the $K^0_S\pi^+\pi^-$ final state, the other in one of several different tag categories. The main principles are outlined below, but most experimental considerations and implementation details are left out for the sake of brevity.

The simplest case is when one D meson decays into a final state that uniquely tags the flavour, such as $\overline{D}^0 \to K^+e^-\bar{\nu}_e$. In that case, the D meson decaying to $K^0_S\pi^+\pi^-$ is known to be in the D^0 state and the decay rate is simply determined by $A^D_S : \Gamma(s_{-+}) \propto |A^D_S(s_{-+})|^2$. This allows for a measurement of the K_i parameters.

If one D meson is reconstructed in a *CP*-even state, eg. K^+K^-, or a *CP*-odd state, eg. $K^0_S\pi^0$, the D meson decaying to $K^0_S\pi^+\pi^-$ is known to be in a state of opposite *CP*. Thus, for a tag-decay of $CP = \pm 1$ the decay rate has the form

$$\Gamma_{CP=\pm1} \propto \left|A^D_S(s_{-+}) \mp A^D_S(s_{+-})\right|^2 \tag{1.29a}$$

and the bin yields will be given by

$$M^\pm_i \propto K_i + K_{-i} \mp 2\sqrt{K_iK_{-i}}c_i. \tag{1.29b}$$

Thus a simultaneous analysis of flavour and *CP* tagged decays allow for a determination of the K_i and c_i parameter sets.

Finally, the case where both D mesons, for now denoted D and D', decay into the $K^0_S\pi\pi$ final state can be considered. The total amplitudes have contributions from the case where D is in the D^0 state and D' is in the $\overline{D}^0$ state, as well as the opposite flavour assignment. Thus the decay rate satisfies

$$\Gamma_{CP=\pm1} \propto \left|A^D_S(s_{-+})A^D_S(s'_{+-}) + A^D_S(s_{+-})A^D_S(s'_{-+})\right|^2 \tag{1.30a}$$

where s_{-+} denotes the Dalitz-plot coordinates of the D meson, and s'_{-+} those of the D' meson. Defining M_{ij} to be the yield of decays where the D decay is in bin i and the D' in bin j, the bin yields satisfy

$$M_{ij} \propto K_iK_{-j} + K_jK_{-i} - 2\sqrt{K_iK_{-i}K_jK_{-j}}\,(c_ic_j + s_is_j)\,. \tag{1.30b}$$

Thus, analysing these decays in addition to the *CP* and flavour tagged decays provide information on all of K_i, c_i, and s_i. Note, however, that Eqs. (1.29) and (1.30) are invariant under the transformation $\delta_D \to -\delta_D$. In practice, the analysis is extended in a number of ways to enhance the statistics: using "flavour-tag" states that are not exact flavour tags, such as $K^-\pi^+$, using self-conjugate multi-body D-decay final states that are not exact *CP* eigenstates, such as $\pi^+\pi^-\pi^0$, and using the $K^0_L\pi^+\pi^-$ final state as well. However, the main principles are the same as described above.

Where exactly is this phase sign know from? Is the overall sign not arbitrary in amplitude models?

The measurements of c_i and s_i are made for a range of different binning schemes. It was noted already in Ref. [?] that a rectangular binning scheme, such as the example in Fig. 1.6, does not provide the optimal sensitivity to γ. A better sensitivity can be obtained if the bins are defined such that δ_D is approximately constant over a given bin, by defining bin i out of N via the condition

$$\text{bin}_i = \{(s_-, s_+) \quad | \quad 2\pi(i - 3/2)/N \, < \, \delta_D(s_-, s_+) \, < \, 2\pi \times (i - 1/2)/N\} \, . \quad (1.31)$$

In practice, the binning scheme is defined by splitting the D-decay phase-space into quadratic *micro bins* with a width of 0.0054 $(\text{GeV}/c^2)^2$ and assigning a bin number to each micro bin via the condition in (1.31) as evaluated in an amplitude model of choice. The obtained binning scheme when using an amplitude model developed by the BaBar collaboration in 2008 [?] is shown in Fig. 1.7a. In Ref [?] it was also shown that the binning can be even further optimised for sensitivity. The suggested figure of merit is

$$Q^2 = \frac{\sum_i \left(\frac{1}{\sqrt{N_i^B}} \frac{\mathrm{d}N_i^B}{\mathrm{d}x}\right)^2 + \left(\frac{1}{\sqrt{N_i^B}} \frac{\mathrm{d}N_i^B}{\mathrm{d}y}\right)^2}{\int \mathrm{d}s^2 \left[\left(\frac{1}{|\Gamma^B(s_{-+})|} \frac{\mathrm{d}|\Gamma^B(s_{-+})|^2}{\mathrm{d}x}\right)^2 + \left(\frac{1}{|\Gamma^B(s_{-+})|} \frac{\mathrm{d}|\Gamma^B(s_{-+})|^2}{\mathrm{d}y}\right)^2\right]} \quad (1.32)$$

which quantifies the statistical sensitivity for a given binning, relative to the one achievable in an unbinned analysis. The CLEO collaboration defined an *optimal* binning scheme by an iterative procedure where, starting from the equal binning scheme, a micro-bin is randomly reassigned new bin numbers in each step, and a step accepted if Q^2 increases. The optimisation is done for the case where $x = y = 0$ and thus Q^2 simplifies to $Q^2_{x=y=0} = \sum_i N_i^{x=y=0}(c_i^2 + s_i^2)/N_{total}^{x=y=0})$. The resulting binning scheme is shown in Fig. 1.7b. An additional binning scheme is defined, denoted the *modified optimal* scheme and shown in Fig. 1.7c, where the Q^2 figure of merit is modified to take into account the presence of backgrounds [?]. The modified optimal binning scheme has proven beneficial to use in measurements with small signal yields [], but is not employed in the present thesis.

Table 1.1: The experimentally measured c_i and s_i values used in the thesis. The $D \to K^0_S\pi^+\pi^-$ values are the combined values from the BESIII and CLEO measurements published by BESIII [**?**]. The $D \to K^0_S K^+K^-$ values are measured by CLEO [**?**].

Optimal binning scheme: $D \to K^0_S\pi^+\pi^-$		
Bin i	c_i	s_i
1	-0.037 ± 0.049	0.829 ± 0.097
2	0.837 ± 0.067	0.286 ± 0.152
3	0.147 ± 0.066	0.786 ± 0.154
4	-0.905 ± 0.021	0.079 ± 0.059
5	-0.291 ± 0.041	-1.022 ± 0.062
6	0.272 ± 0.082	-0.977 ± 0.176
7	0.918 ± 0.017	-0.184 ± 0.065
8	0.773 ± 0.033	0.277 ± 0.118

2-bins binning scheme: $D \to K^0_S K^+K^-$		
Bin i	c_i	s_i
1	0.818 ± 0.107	-0.445 ± 0.215
2	-0.746 ± 0.083	-0.229 ± 0.220

Both the CLEO and BESIII collaborations have measured the values of c_i and s_i for the equal, optimal, and modified optimal binning schemes. The results are also shown in Fig. 1.7, where they are compared to the expectation from the latest amplitude model [**?**]. The measurements presented in this thesis are based on a combination of the BESIII and CLEO results for the optimal binning scheme, made by the BESIII collaboration [**?**] and tabulated in Table 1.1.

While the *definition* and *optimisation* of these binning schemes depend on knowledge of $A^D_S(s_-, s_+)$ via an amplitude model, it is important to note that no model information is needed when the binning schemes are used in the subsequent measurements of strong-phases[5] or *CP*-observables. Therefore the measurements will not be biased by any modelling imperfections, although the obtained precision might be lower than expected.

The preceding discussion has been focusing on the $D \to K^0_S\pi^+\pi^-$ channel, however the $D \to K^0_S K^+K^-$ channel can be analysed completely analogously. The CLEO collaboration measure c_i and s_i values for this mode as well, in three binning schemes [**?**]. These are all equal-phase binning schemes, with 2, 3, and 4 bins,

[5]With the exception of minimal model-dependence introduced when the $K^0_L\pi^+\pi^-$ final state is employed to constrain the s_i parameters by the D-factories [**?**, **?**], the impact of which is well under control.

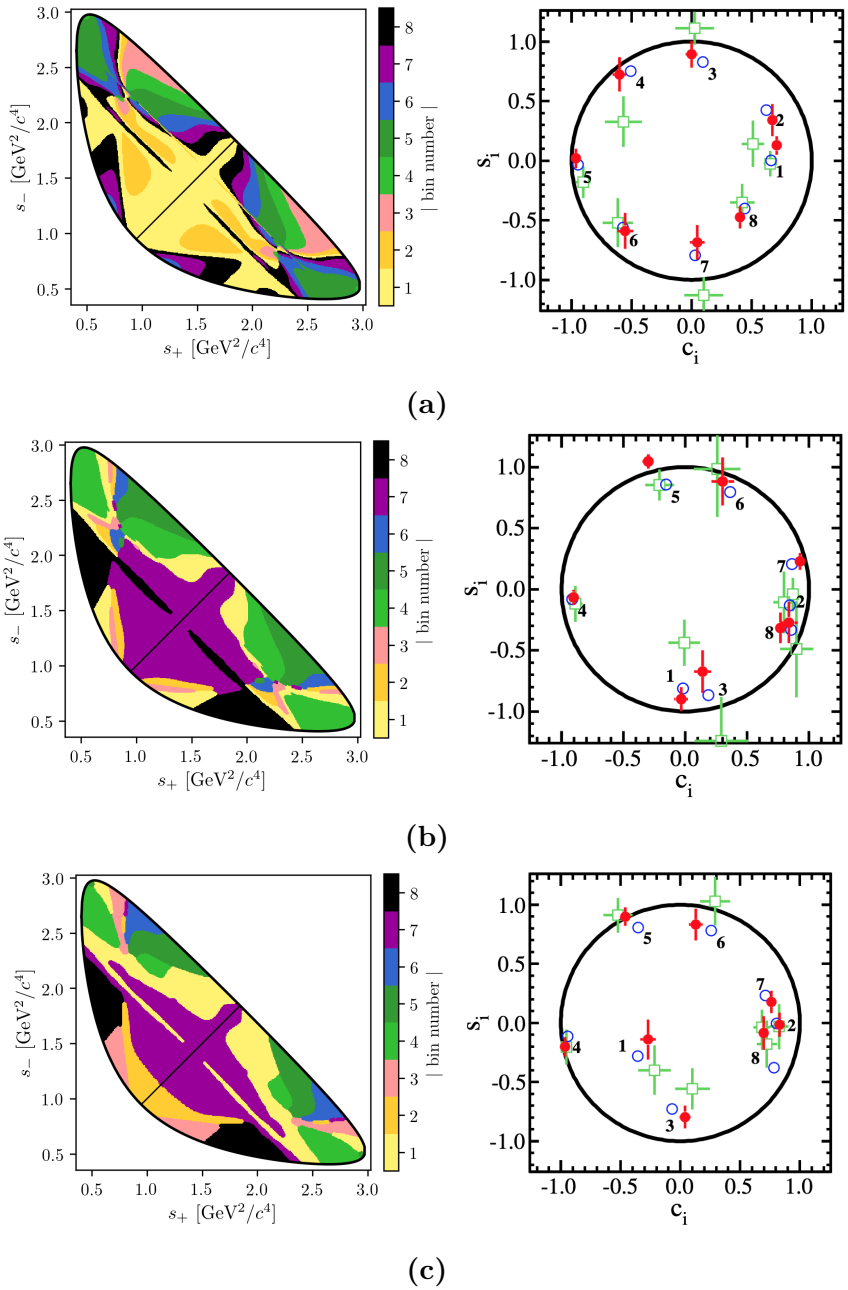

Figure 1.7: The (left) binning schemes and (right) measured values of (c_i, s_i) for (a) equal, (b) optimal, and (c) modified optimal binning schemes for $D \to K^0_S\pi^+\pi^-$. The plots of the measured values are taken from Ref. [**?**] and show the results obtained by (red) BESIII, (green) CLEO, and (blue) the model expectation using the model from Ref. [**?**]. The measurement featured in this thesis used the optimal binning scheme.

respectively, shown in Fig. 1.8. The $D \to K^0_S K^+ K^-$ decay amplitude is almost completely dominated by two K^+K^- resonances, the *CP*-odd $\phi(1020)$ and the *CP*-even $a_0(980)$, and this means that very little gain in sensitivity can be made by altering the equal-phase binning schemes. The measured c_i and s_i values are also shown in Fig. 1.8 and tabulated in Table 1.1 for the 2-bins scheme, which is used in this thesis. A BESIII measurement is in preparation, but has not been finished at the time of writing.

1.3.5 Global CP asymmetry and the relation to GLW and ADS measurements

The introduction of separate normalisation factors h^+ and h^- in Eq. (1.25) hides the fact that information on γ (in principle) can be obtained from the asymmetry in phase-space-integrated B^+ and B^- yields. In the ideal case where $h^- = h^+$ the total yield asymmetry is

$$\begin{aligned} A_{GGSZ} &= \frac{\sum_i N^-_- - N^+_i}{\sum_{i=-N}^{N} N^- i - + N^+_i} = \frac{\sum_{i=-N}^{N} \sqrt{K_i K_{-i}} c_i (x_- - x_+)}{1 + r_B^2 + 2\sum_{i=-N}^{N} \sqrt{K_i K_{-i}} c_i (x_- + x_+)} \\ &= \frac{2\sum_{i=1}^{N} \sqrt{K_i K_{-i}} c_i (x_- - x_+)}{1 + r_B^2 + 4\sum_{i=1}^{N} \sqrt{K_i K_{-i}} c_i (x_- + x_+)}, \end{aligned} \tag{1.33}$$

where it has been exploited that $\sum_{i=-N}^{N} \sqrt{K_i K_{-i}} s_i = 0$ by definition. The size of the asymmetry is governed by the factor $\sum_{i=1}^{N} \sqrt{K_i K_{-i}} c_i$, which is small for $D \to K^0_S \pi^+ \pi^-$ and $D \to K^0_S K^+ K^-$ decays. The underlying reason is that $\delta_D(s_-, s_+)$ varies significantly across phase-space for these decays, as evident by the spread in the values of c_i in Table 1.1, which reduces the *average* of the asymmetry-generating D^0–$\overline{D}^0$ interference term to being close to zero. The value of $\sum_{i=-N}^{N} \sqrt{K_i K_{-i}} c_i$ is closely related to the *CP* content of the final state in question: for a self-conjugate *CP* even (odd) final state

$$A_{D^0}(s_-, s_+) = {}^{+}_{(-)} A_{\overline{D}^0}(s_-, s_+) = {}^{+}_{(-)} A_{D^0}(s_+, s_-) \tag{1.34}$$

and thus $\sum_{i=1}^{N} \sqrt{K_i K_{-i}} c_i = {}^{+}_{(-)} 1$. This motivates the definition of the *CP*-even fraction of the decay

$$\mathcal{F}_+ \equiv \frac{1}{2} \left(1 + \sum_{i=1}^{N} \sqrt{K_i K_{-i}} c_i \right). \tag{1.35}$$

With $\mathcal{F}_+$ in hand, the asymmetry in Eq. (1.33) can be rewritten

$$A_{GGSZ} = \frac{(2\mathcal{F}_+ - 1) r_B \sin\delta_B \sin\gamma}{1 + r_B^2 (2\mathcal{F}_+ - 1) 2 r_B \cos\delta_B \cos\gamma}, \tag{1.36}$$

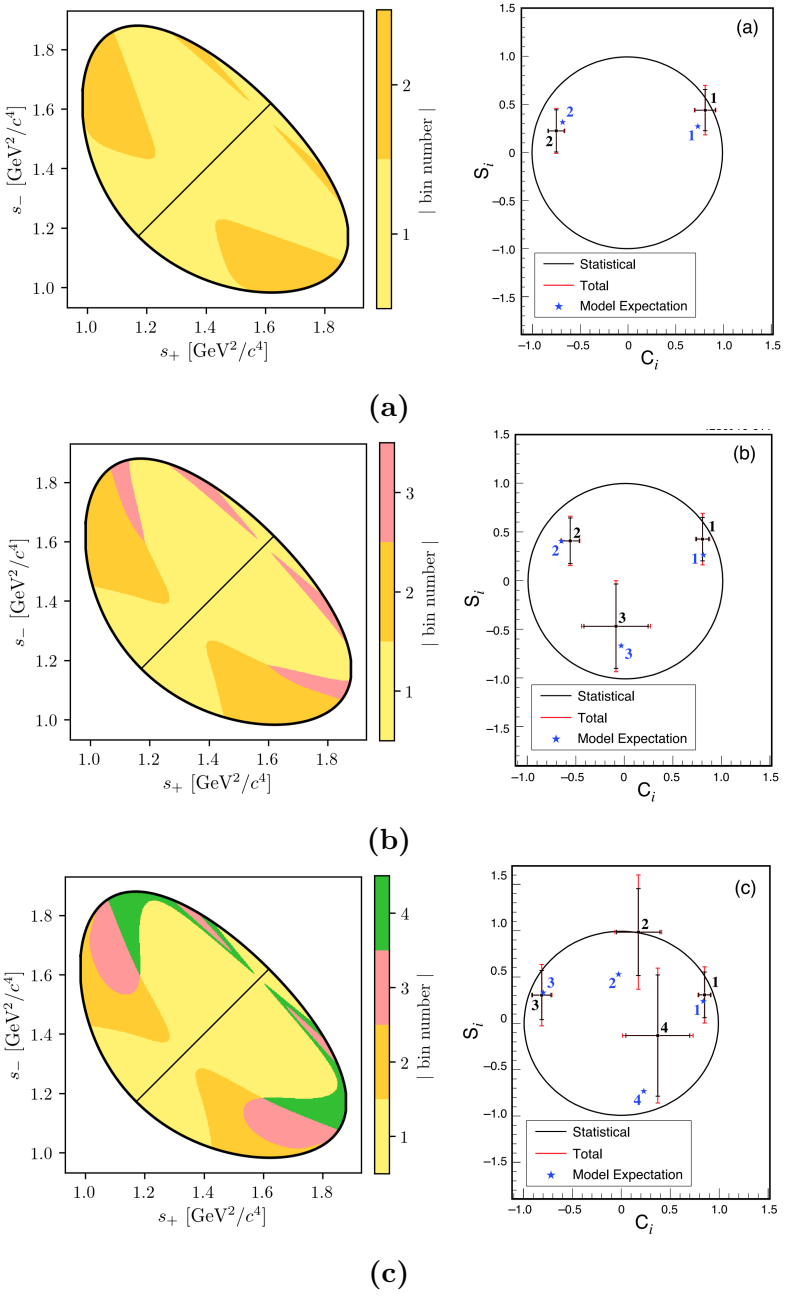

Figure 1.8: The (left) binning schemes and (right) measured values of (c_i, s_i) for the (a) 2-, (b) 3-, and (c) 4-bins binning schemes for $D \to K^0_S K^+ K^-$. The plots of the measured values are taken from Ref. [**?**] and show the (error bars) results obtained by CLEO, and (blue) the model expectation using the model from Ref. [**?**]. The measurement featured in this thesis uses the 2-bins scheme.

which is the usual form used in quasi-GLW measurements []; for $N = 1$ the definition in Eq. (1.35) is equivalent to $\mathcal{F}_+$ as defined in Ref. []. The value of $\mathcal{F}_+$ is independent of the number and shape of bins in a given binning scheme, as long as the bin definitions follow the symmetry principles outlined in Section 1.3.3. For $D \to K^0_S\pi^+\pi^-$ and Å decays the values of $\mathcal{F}_+$ are

$$\begin{aligned} \mathcal{F}_+(K^0_S\pi^+\pi^-) &= X? \\ \mathcal{F}_+(K^0_S K^+K^-) &= X? \end{aligned} \tag{1.37}$$

as evaluated with the Belle 2018 model for $D \to K^0_S\pi^+\pi^-$ decays and the BaBar 2010 model for $D \to K^0_S K^+K^-$ decays. Since $r_B^{DK^\pm} \sim 0.1$ the predicted global asymmetries are thus approximately 1–2 %, which is not resolvable with the current experimental yields. As shown in Chapter 3, *CP* violation in the K^0_S sector leads to asymmetries of a similar size, further complicating the use of global asymmetries to constrain $x_\pm$ and $y_\pm$. Thus these modes are ill-suited for quasi-GLW measurements, and ignoring global asymmetries leads to a negligible loss of information on γ in a GGSZ measurement. The reverse is true for a well-suited quasi-GLW mode, such as $D \to \pi^+\pi^-\pi^0$: if $\mathcal{F}_+$ is close to either zero or unity, it means that (c_i, s_i) will be close to $(\pm 1, 0)$ in all bins for *any* given binning scheme, and the set of bins will provide almost identical constraints on $x_\pm$ and $y_\pm$. Thus, the binning of phase space leads to no significant gain in precision compared to a global analysis.

Indeed, a crucial quality of the GGSZ method, is that exactly because each bin-pair provides independent constraints on $x_\pm$ and $y_\pm$, the method provides a single solution for (γ, r_B, δ_B) that does not suffer the ambiguities of the ADS and GLW approaches. In order to illustrate this further, it is useful to make one more comparison of the model-independent GGSZ formalism to the ADS and GLW formalisms. If there was no *CP* symmetry the B^+ yield in bin $+i$ would equal the B^- yield in bin $-i$. Therefore the relevant *CP* asymmetry for a given Dalitz bin is

$$\begin{aligned} A^i_{GGSZ} &\equiv \frac{N^-_i - N^+_{-i}}{N^-_i + N^+_{-i}} \\ &= \frac{\sqrt{K_i K_{-i}}(c_i(x_- - x_+) + s_i(y_- - y_+))}{K_i + r_B^2 K_{-i} + 2\sqrt{K_i K_{-i}}(c_i(x_- + x_+) + s_i(y_- + y_+))}. \end{aligned} \tag{1.38}$$

This expression is identical to the ADS asymmetry in Eq. (1.16a) if the effective D-decay parameters r^i_D and δ^i_D are defined via

$$\kappa_i \cos\delta^i_D \equiv c_i \qquad , \qquad \kappa_i \sin\delta^i_D \equiv s_i \qquad , \qquad r^i_D \equiv \sqrt{K_i/K_{-i}}, \tag{1.39}$$

and a coherence factor, κ, is included in the interference terms of the ADS expression, as is standard for multi-body D decays []. These parameters allow us to classify

Table 1.2: Classification of the bins used in model-independent GGSZ measurements, in terms of whether the interplay between the D^0 and $\overline{D}^0$ amplitudes in the bin resemble typical GLW or ADS behaviour. The parameters are calculated using the 2018 Belle model [] for $D \to K^0_S\pi^+\pi^-$ decays and the 2010 BaBar model [] for $D \to K^0_S K^+K^-$ decays.

Optimal binning scheme: $D \to K^0_S\pi^+\pi^-$					
Bin i	$\hat{r}_D$	$\hat{\delta}_D$	$\mathcal{F}_+$	κ	Bin type
1	0.473	91.9°	48.97 %	0.81	Mixed
2	0.164	11.1°	63.38 %	0.85	ADS-like
3	0.157	79.4°	52.50 %	0.89	ADS-like
4	0.768	175.3°	5.85 %	0.92	GLW-odd-like
5	0.759	−99.9°	42.84 %	0.87	Mixed
6	0.223	−64.5°	57.92 %	0.87	ADS-like
7	0.651	−13.3°	89.44 %	0.89	GLW-even-like
8	1.745	21.0°	87.08 %	0.92	GLW-even-like

2-bins binning scheme: $D \to K^0_S K^+K^-$					
Bin i	$\hat{r}_D$	$\hat{\delta}_D$	$\mathcal{F}_+$	κ	Bin type
1	0.816	19.8°	86.14 %	0.78	GLW-even-like
2	0.775	154.5°	16.23 %	0.77	GLW-odd-like

a given pair of bins with number $\pm i$ as either *GLW-like*, if δ^i_D is close to 0 or π and r^i_D is close to unity, or *ADS-like* if $0 < r^i_D \ll 1$. The *CP*-even fraction of the D-decay can also be defined for a given bin-pair:

$$\mathcal{F}^i_+ = \mathcal{F}^{-i}_+ \equiv \frac{1}{2}\left(1 + 2c_i\frac{\sqrt{K_i K_{-i}}}{K_i + K_{-i}}\right) = \frac{1}{2}\left(1 + 2c_i\frac{r^i_D}{1 + {r^i_D}^2}\right). \tag{1.40}$$

A GLW-even-like bin pair will have $\mathcal{F}^i_+ \simeq 1$ and a GLW-odd-like bin pair will have $\mathcal{F}^i_+ \simeq 0$.

Table 1.2 summarises a classification of the bins for the optimal $D \to K^0_S\pi^+\pi^-$ binning scheme and the 2-bins $D \to K^0_S K^+K^-$ binning scheme following these principles. Two bins are classified as *mixed* because r^i_D is not particularly small, but $\mathcal{F}^i_+$ is close to 0.5. The fact that multiple bin types appear for both the $D \to K^0_S\pi^+\pi^-$ and $D \to K^0_S K^+K^-$ modes underline that each mode benefits from being analysed in the GGSZ formalism, and that the bins provide independent constraints, allowing for a non-ambiguous solution for (γ, r_B, δ_B).

1.4 Strategy for the LHCb measurement

The main topic of the thesis is a model-independent GGSZ measurement using $B^\pm \to DK^\pm$ and $B^\pm \to D\pi^\pm$ decays, and the two D final states $K^0_S\pi^+\pi^-$ and $K^0_S K^+K^-$. The measurement uses the optimal binning scheme for the $D \to K^0_S\pi^+\pi^-$ mode, with the combined strong-phase inputs from the BESIII [**?**] and CLEO [**?**] collaborations published in Ref. [**?**]. For the $D \to K^0_S K^+K^-$ channel, the 2-bins scheme is used with the strong-phase parameters measured by the CLEO collaboration [**?**]. The details of the analysis are presented in Chapter (4), but the overall strategy and a few extensions of the formalism from the previous sections are given here.

Due to the geometry of the LHCb detector, the signal reconstruction efficiency for $B^\pm \to D(\to K^0_S h^+h^-)h'^\pm$ decays varies significantly across the D-decay phase space. Denoting the efficiency profile as $\eta(s_-, s_+)$, the yield equations of Eq. (1.25) are therefore modified slightly

$$\begin{aligned} N_i^- &= h^{B^-}\left[F_i + r_B^2 F_{-i} + 2\sqrt{F_i F_{-i}}\,(c'_i x_- + s'_i y_-)\right], \\ N_i^+ &= h^{B^+}\left[F_{-i} + r_B^2 F_i + 2\sqrt{F_i F_{-i}}\,(c'_i x_+ - s'_i y_+)\right], \end{aligned} \tag{1.41}$$

where the phase-space integrated quantities now include the efficiency profile

$$F_i = \frac{1}{N_F}\int_i \mathrm{d}s^2\,\eta(s_{-+})|A^D_S(s_{-+})|^2, \qquad N_F = \int \mathrm{d}s^2\,\eta(s_{-+})|A^D_S(s_{-+})|^2, \tag{1.42}$$

$$c'_i = \frac{\int_i \mathrm{d}s^2\,\eta(s_{-+})|A^D_S(s_{-+})||A^D_S(s_{+-})|\cos[\delta_D(s_{-+})]}{\sqrt{\int_i \mathrm{d}s^2\,\eta(s_{-+})|A^D_S(s_{-+})|^2}\sqrt{\int_i \mathrm{d}s^2\,\eta(s_{-+})|A^D_S(s_{+-})|^2}}, \tag{1.43}$$

with an analogous definition of s'_i. At leading order, the strong-phase parameters are unaffected by the non-uniform efficiency, and, in addition, the bin definitions favour bins for which c_i and s_i take on similar values across each bin. Therefore, the c_i and s_i values reported by the charm factories are used directly in the measurement. The impact on the obtained central values is negligible, as described in detail in Section 4.5 where a systematic uncertainty is assigned.

The F_i *are* significantly different to the K_i due to the experimental acceptance profile in LHCb. Given external inputs for the strong-phase parameters, it is possible to fit the F_i parameters *and* $x_\pm$ and $y_\pm$ simultaneously in a fit to the LHCb $B^\pm \to DK^\pm$ data set, in which case the obtained F_i parameters incorporate the correct acceptance profile correction by construction. However, the obtainable precision for the *CP* observables measured by this procedure is suboptimal. As

an alternative, the first LHCb measurement [**?**] made a simultaneous analysis of $B^\pm \to DK^\pm$ and a much larger sample of $B^\pm \to D\pi^\pm$ decays; since the F_i parameters relate to the D decay, they can effectively be obtained in the $D\pi^\pm$ sample and shared between the two $B^\pm \to Dh^\pm$ channels. However, there is *CP* violation present in the $B^\pm \to D\pi^\pm$ decays, which led to a dominant systematic uncertainty. Later LHCb measurements [**?**, **?**] instead relied on flavour tagged D mesons from $\overline{B}^0 \to D^{*+}(\to D^0\pi^+)\mu^-\bar{\nu}_\mu X$ decays to obtain F_i, where no *CP* violation in possible. However, due to necessarily different triggering paths and selections, the acceptance profile is not exactly identical between semi-leptonic decays and the $B^\pm \to Dh^\pm$ decays of interest. An efficiency correction based on simulation was therefore applied to obtain the correct F_i, and in this case, the uncertainty related to the correction constituted the largest systematic uncertainty on the measurement.

Both sources of systematic uncertainty can be avoided by making a simultaneous analysis of $B^\pm \to DK^\pm$ and $B^\pm \to D\pi^\pm$ decays, where *CP*-violating observables are measured in *both* channels and the F_i parameters are shared. Effectively, the F_i are determined in the high statistics $B^\pm \to D\pi^\pm$ channel, but with no systematic effect from *CP*-violation in that channel, since the *CP*-violation is incorporated in the yield description. At the start of the work that lead to this thesis, it was not clear to what degree the measured *CP*-violating observables in $B^\pm \to D\pi^\pm$ decays were affected by *CP* violation in the neutral kaon sector. The impact had been shown to scale as $\mathcal{O}(|\epsilon|/r_B)$ [**?**], which is negligible for the $B^\pm \to DK^\pm$ channel but suggests potentially large biases in the $B^\pm \to D\pi^\pm$ channel, where r_B is 20 times smaller. However, the dedicated analysis presented in Chapter 3 has proved the effect on GGSZ measurements to be in fact be *smaller* than $\mathcal{O}(|\epsilon|/r_B)$ and the simultaneous measurement is indeed viable.

The measurement is performed by making extended maximum-likelihood fits to the m_B spectra of $B \to D(\to K^0_S h^+h^-)h'^\pm$ candidates split by charge and Dalitz bin. The $B^\pm \to DK^\pm$ signal yields are parameterised using the expressions in Eq. (1.41) directly, thus obtaining values for $x^{DK}_\pm$ and $y^{DK}_\pm$ directly. The Cartesian *CP*-violating observables $x_\pm$ and $y_\pm$ are employed because they lead to better statistical behaviour than fits to data where the underlying parameters $(\gamma, r_B^{DK^\pm}, \delta_B^{DK^\pm})$ are determined [], at the cost of introducing a fourth degree of freedom. With the addition of the $B^\pm \to D\pi^\pm$ mode as a true signal channel, two new underlying parameters are introduced, $r_B^{D\pi^\pm}$ and $\delta_B^{D\pi^\pm}$. It is only necessary to introduce an additional two, not four, Cartesian parameters [**?**] by defining

$$\xi_{D\pi^\pm} = \left(\frac{r_B^{D\pi^\pm}}{r_B^{DK^\pm}}\right) \exp[i(\delta_B^{D\pi^\pm} - \delta_B^{DK^\pm})] \tag{1.44a}$$

and letting

$$x_\xi^{D\pi} = \mathrm{Re}[\xi_{D\pi^\pm}] \qquad\qquad y_\xi^{D\pi} = \mathrm{Im}[\xi_{D\pi^\pm}]. \tag{1.44b}$$

In terms of these parameters, the usual Cartesian $x_\pm$ and $y_\pm$ are given by

$$x_\pm^{D\pi} = x_\xi^{D\pi} x_\pm^{DK} - y_\xi^{D\pi} y_\pm^{DK}, \qquad y_\pm^{D\pi} = x_\xi^{D\pi} y_\pm^{DK} + y_\xi^{D\pi} x_\pm^{DK}. \tag{1.45}$$

Using this expression, the $B^\pm \to D\pi^\pm$ yields can also be defined via Eq. (1.41) in the maximum-likelihood fit. This allows for a stable fit for all six x and y parameters, as well as the shared F_i, as described in much greater detail in Chapter 4. Note that ξ does not depend on γ: all information on *CP* asymmetries in both the $B^\pm \to DK^\pm$ and $B^\pm \to D\pi^\pm$ channels is encoded in $x_\pm^{DK}$ and $y_\pm^{DK}$.

The combined analysis of $B^\pm \to DK^\pm$ and $B^\pm \to D\pi^\pm$ decays presents a significant step forward, because it solves the problem of obtaining F_i parameters for the appropriate acceptance profile in a manner that avoids leading systematic uncertainties, and almost all reliance on simulation. This is of great importance, if the large data samples that will be collected by LHCb in the future are to be exploited to their full potential.

2

The LHCb experiment

We have a detector? I thought ntuples were made of magic.

2.1 Subdetectors

2.1.1 The VELO

2.1.2 Magnet and tracking stations

2.1.3 The RICH

2.1.4 Calorimeters

2.1.5 Muon detectors

2.2 Track reconstruction

2.3 The LHCb triggerring system

2.3.1 The level-0 hardware trigger

2.3.2 High-level triggers

2.3.3 Offline data filtering: the LHCb stripping

2.4 Simulation

Include a short description of RapidSim.

3

Neutral kaon *CP* violation and material interaction in BPGGSZ measurements

The presence of a K^0_S meson in the $D \to K^0_S h^+ h^-$ final states introduces a small bias in BPGGSZ measurements due to *CP*-violation in the neutral kaon sector and asymmetries caused by the interaction between the neutral kaons and detector material. These fundamental physics effects are reviewed in Section 3.1, after which the chapter presents a detailed analysis of the impact on the LHCb measurement that is the subject of the thesis, as well as future γ measurements with the Belle II experiment. Prior to this analysis, the only existing work on the the effect on γ measurements suggested a small effect in $B^\pm \to DK^\pm$ measurements but potentially *very* significant effects in measurements based on $B^\pm \to D\pi^\pm$ decays [**?**]. However, as described in Section 3.1.1, the analysis in Ref. [**?**] does not take into account the fundamental aspect of the BPGGSZ method: that it relies on the phase-space distribution of signal decays, not phase-space integrated asymmetries. Furthermore, the study only considers the *CP*-violation effect, not material interaction. Therefore, a more detailed study was necessary before the $B^\pm \to D\pi^\pm$ decay mode could reliably be promoted to a signal channel.

3.1 CP violation and material interaction of neutral kaons

A brief review of the general phenomenology of mixing and *CP* violation in the neutral kaon system is useful, before analysing the impact on γ measurements.

The presentation in this section follows the PDG review of *CP violation in the quark section* [**?**]. The general theory considers any pair of neutral mesons $|M^0\rangle$ and $|\overline{M}^0\rangle$ related by CP conjugation

$$CP|M^0\rangle = e^{i\phi_M}|\overline{M}^0\rangle \qquad CP|\overline{M}^0\rangle = e^{-i\phi_M}|M^0\rangle, \tag{3.1a}$$

where ϕ_M is an arbitrary phase. In this thesis, the convention $\phi_M = 0$ is chosen to equal zero, so that

$$CP|M^0\rangle = |\overline{M}^0\rangle \qquad CP|\overline{M}^0\rangle = |M^0\rangle. \tag{3.1b}$$

A meson state that starts as a general superposition of $|M^0\rangle$ and $|\overline{M}^0\rangle$ states

$$\begin{aligned} \psi_M^0 \equiv \psi_M(0) &= a(0)|M^0\rangle + b(0)|\overline{M}^0\rangle \\ &\equiv \psi_{M^0}^0 + \psi_{\overline{M}^0}^0 \end{aligned} \tag{3.2}$$

will, over time, involve into a state that consists of a different superposition of $|M^0\rangle$ and $|\overline{M}^0\rangle$, as well as components for all possible states the meson system can decay into

$$\begin{aligned} \psi_M(t) &= a(t)|M^0\rangle + b(t)|\overline{M}^0\rangle + \sum c_i(t) f_i \\ &\equiv \psi_{M^0}(t) + \psi_{\overline{M}^0}(t) + \sum c_i(t) f_i. \end{aligned} \tag{3.3}$$

For time scales that are longer than the typical strong-interaction, the time evolution of the M^0–$\overline{M}^0$ superposition can be described by a 2×2 Hamiltonian

$$\frac{\mathrm{d}}{\mathrm{d}t}\begin{pmatrix}\psi_{M^0}(t)\\ \psi_{\overline{M}^0}(t)\end{pmatrix} = -i\mathcal{H}_0\begin{pmatrix}\psi_{M^0}(t)\\ \psi_{\overline{M}^0}(t)\end{pmatrix} \tag{3.4}$$

that is *non-Hermitian* (to allow for decay) but can be parameterised in terms of two Hermitian matrices $\mathcal{M}$ and Γ_0

$$\mathcal{H}_0 = \mathcal{M} - \frac{i}{2}\Gamma_0. \tag{3.5}$$

The quantum states with well-defined (real) masses, m_j, and (real) decay widths, Γ_j, are the two eigenstates of $\mathcal{H}_0$ with eigenvalues $\lambda_j = m_j - \frac{i}{2}\Gamma_j$. The eigenstates (of course) evolve independently in time, so that

$$\psi_j(t) = e^{-i\lambda_j t}\psi_j^0 = e^{-im_j t - \frac{\Gamma_j}{2}t}\psi_j^0. \tag{3.6}$$

The eigenstates are denoted H and L according to the size of m_j, the real part of the eigenvalues, such that $m_H > m_L$. Assuming that $\mathcal{H}_0$ conserves CPT the eigenstates have the general form

$$\begin{aligned} |M_H\rangle &\equiv p|M^0\rangle - q|\overline{M}^0\rangle \\ |M_L\rangle &\equiv p|M^0\rangle + q|\overline{M}^0\rangle \end{aligned} \tag{3.7}$$

where p and q are complex numbers that satisfy $|q|^2 + |p|^2 = 1$. With the convention in Eq. (3.1b) it follows that *if* $\mathcal{H}_0$ also conserves *CP*, so that $|M_H\rangle$ and $|M_L\rangle$ are *CP* eigenstates, then $p = \pm q$, where the sign depends on which of the heavy and the light meson states is *CP* even, and which is *CP* odd.

The eigenstates of the Hamiltonian governing the neutral kaon system are almost, but not exactly, equal to the *CP* eigenstates

$$|K_1\rangle = \frac{|K^0\rangle + |\overline{K}^0\rangle}{\sqrt{2}} \qquad |K_2\rangle = \frac{|K^0\rangle - |\overline{K}^0\rangle}{\sqrt{2}}, \tag{3.8}$$

which are *CP* even and odd, respectively. This approximate equality leads to the most prominent feature of the neutral kaon system: the two eigenstates of $\mathcal{H}_0$ have lifetimes that differ by orders of magnitude. This is best understood by assuming, for a moment, that the states in Eq. (3.8) *do* equal the eigenstates with definite life times. The K_1 state can decay in the *CP* even $\pi^+\pi^-$ and $\pi^0\pi^0$ modes, and does so almost 100 % of the time; these decay modes are not available to the K_2 (in the absence of direct *CP* violation) which results in a much lower decay rate and much longer life time. Therefore, the eigenstates in the kaon system are labelled the *short-lived* kaon, K^0_S, which is almost *CP* even, and the *long-lived* kaon, K^0_L, which is almost *CP* odd. The life times are [**?**]

$$\tau_{K^0_\mathrm{S}} = (8.954 \pm 0.004) \times 10^{-11}\mathrm{s} \qquad \tau_{K^0_\mathrm{L}} = (5.116 \pm 0.021) \times 10^{-8}\mathrm{s}. \tag{3.9}$$

Experimentally, it is found that the K^0_S corresponds to the light eigenstate, but that the mass splitting [**?**]

$$\begin{aligned} \Delta m = m_{K^0_\mathrm{L}} - m_{K^0_\mathrm{S}} &= (0.5289 \pm 0.0009) \times 10^{10}\,\hbar\mathrm{s}^{-1} \\ &\simeq 3.5 \times 10^{-6}\,\mathrm{eV} \end{aligned} \tag{3.10}$$

is tiny compared to the neutral kaon masses of $m_{K^0_\mathrm{S}} = 497.6\,\mathrm{MeV}/c^2$ [**?**].

However, the discovery of $K^0_\mathrm{L} \to \pi\pi$ decays by Kronin and Fitch in 1964 established that the K^0_S and K^0_L are *not* exactly equal to the *CP* eigenstates in Eq. (3.8), because the $\mathcal{H}_0$ relevant to the kaon system is *CP*-violating. The *CP* violation in the kaon sector is conventionally parameterised in terms of the complex parameters ϵ and ϵ', in terms of which

$$\frac{A(K^0_\mathrm{L} \to \pi^+\pi^-)}{A(K^0_\mathrm{S} \to \pi^+\pi^-)} = \epsilon + \epsilon' \qquad \frac{A(K^0_\mathrm{L} \to \pi^0\pi^0)}{A(K^0_\mathrm{S} \to \pi^0\pi^0)} = \epsilon - 2\epsilon'. \tag{3.11}$$

In these expressions ϵ denotes the contribution from *CP* violation in mixing and ϵ' the contribution due to direct *CP* violation in the decays. The ϵ parameter has been measured to be [**?**]

$$|\epsilon| = (2.228 \pm 0.011) \times 10^{-3}, \qquad \arg\epsilon = (43.52 \pm 0.05)^\circ. \tag{3.12}$$

Direct *CP* violation is ignored for the remainder of the thesis, because ϵ' is measured to be three orders of magnitude smaller than ϵ. In terms of the *CP* eigenstates of Eq. (3.8), the mass eigenstates K^0_{S} and K^0_{L} are given by

$$\begin{aligned} |K^0_{\mathrm{S}}\rangle &= \frac{|K_1\rangle + \epsilon|K_2\rangle}{\sqrt{1+|\epsilon|^2}} &&= \frac{(1+\epsilon)|K^0\rangle + (1-\epsilon)|\overline{K}^0\rangle}{\sqrt{2(1+|\epsilon|^2)}} \\ |K^0_{\mathrm{L}}\rangle &= \frac{|K_2\rangle + \epsilon|K_1\rangle}{\sqrt{1+|\epsilon|^2}} &&= \frac{(1+\epsilon)|K^0\rangle - (1-\epsilon)|\overline{K}^0\rangle}{\sqrt{2(1+|\epsilon|^2)}}, \end{aligned} \tag{3.13}$$

corresponding to the definition $p = (1+\epsilon)/\sqrt{2(1+|\epsilon|^2)}$ and $q = (1-\epsilon)/\sqrt{2(1+|\epsilon|^2)}$ in Eq. (3.7).

In an experimental setting, the time evolution of a neutral kaon state is affected by nuclear interactions with the detector. The interaction is governed by the strong force, and therefore sensitive to the *flavour* of the kaon state; the interaction strength is thus different for K^0 and $\overline{K}^0$ mesons. This difference introduces a non-zero $K^0_{\mathrm{S}} \leftrightarrow K^0_{\mathrm{L}}$ transition amplitude for neutral kaons traversing a detector segment. This effect was predicted early in the history of kaon physics [**?**] and is commonly denoted *kaon regeneration*. The effect can be described by including a material-interaction term in the Hamiltonian that is diagonal in the $(|K^0\rangle, |\overline{K}^0\rangle)$ basis, so that the equation governing the time evolution is [**?**, **?**]

$$\frac{\mathrm{d}}{\mathrm{d}t}\begin{pmatrix}\psi_{K^0}(t)\\ \psi_{\overline{K}^0}(t)\end{pmatrix} = -i\left[\mathcal{H}_0 + \begin{pmatrix}\chi & 0\\ 0 & \bar{\chi}\end{pmatrix}\right]\begin{pmatrix}\psi_{K^0}(t)\\ \psi_{\overline{K}^0}(t)\end{pmatrix}. \tag{3.14}$$

The complex parameters χ and $\bar{\chi}$ describe the material interaction of the K^0 and $\overline{K}^0$ flavour eigenstates and are related to their scattering cross section, as described further in Section 3.3.4. The solution of Eq. (3.14) for the time evolution in the K^0_{S} and K^0_{L} states is [**?**]

$$\begin{aligned} \psi_{\mathrm{S}}(t) &= e^{-i\Sigma t}\left(\psi^0_{\mathrm{S}}\cos\Omega t + \frac{i}{2\Omega}\left(\Delta\lambda\psi^0_{\mathrm{S}} - \Delta\chi\psi^0_{\mathrm{L}}\right)\sin\Omega t\right), \\ \psi_{\mathrm{L}}(t) &= e^{-i\Sigma t}\left(\psi^0_{\mathrm{L}}\cos\Omega t - \frac{i}{2\Omega}\left(\Delta\lambda\psi^0_{\mathrm{L}} + \Delta\chi\psi^0_{\mathrm{S}}\right)\sin\Omega t\right), \end{aligned} \tag{3.15}$$

in terms of the parameters

$$\begin{aligned} \Delta\chi &= \chi - \bar{\chi}, \\ \Delta\lambda &= \lambda_{\mathrm{L}} - \lambda_{\mathrm{S}} = (m_{\mathrm{L}} - m_{\mathrm{S}}) - \frac{i}{2}(\Gamma_{\mathrm{L}} - \Gamma_{\mathrm{S}}), \\ \Sigma &= \frac{1}{2}\left(\lambda_{\mathrm{S}} + \lambda_{\mathrm{L}} + \chi + \bar{\chi}\right), \\ \Omega &= \frac{1}{2}\sqrt{\Delta\lambda^2 + \Delta\chi^2}. \end{aligned} \tag{3.16}$$

In the vacuum limit where $\chi = \bar{\chi} = 0$, the expressions in Eq. (3.6) and Eq. (3.15) are equal.

3.1.1 A first look at the impact on γ measurements

The effects described above have an impact on measurements of *CP* asymmetries in modes with a neutral kaon in the final state. This was analysed for the first time in relation to γ measurements by Grossman and Savastio in 2014 [**?**]. The authors point out two sources of corrections to be included:

- the fact that K^0_S is not an exact *CP* eigenstate can break potential symmetry relations employed in an analysis, and
- that when the neutral kaon is reconstructed in a $\pi\pi$ final state there will be contributions from both K^0_S and K^0_L decays.

The analysis in this chapter considers yet another effect, not treated by Grossman and Savastio, namely that

- material interaction can emulate the effect of neutral kaon *CP* violation, because it couples the almost-*CP*-even K^0_S and the almost-*CP*-odd K^0_L states.

Due to the presence of $K^0_L \to \pi\pi$ decays, Grossman and Savastio point out that the relevant decay rates to consider in an experimental setting are of the form

$$\mathrm{d}\Gamma(t) \propto \left|\psi_S(t) + \epsilon\psi_L(t)\right|^2 . \tag{3.17}$$

The time dependence of the decay rates considered in Chapter 1 was left out because all terms shared a common time dependence. That is not the case in Eq. (3.17), due to the very different decay rates of the K^0_S and K^0_L components of the kaon state. As a consequence, the time-integrated yields have the form

$$N \propto \int \mathrm{d}t\, \eta(t) \left|\psi_S(t) + \epsilon\psi_L(t)\right|^2 , \tag{3.18}$$

where $\eta(t)$ is the time acceptance in a given experimental setting. Thus, the acceptance is crucial to model in order to correctly estimates the impact of kaon *CP*-violation effects on a given measurement.

Considering BPGGSZ measurements, the main effect of neutral kaon *CP* violation is a breakdown of the fundamental Dalitz-plot symmetry that is exploited in the derivation of the bin yield equations. Extending the amplitude definition of Eq. (1.21) to include K^0_L decays

$$A^{(\overline{D})}_{S(L)}(s_-, s_+) = A(\,{}^{(\overline{D})^0} \to K^0_{S(L)}\pi^+\pi^-), \tag{3.19}$$

the authors point out that *CP*-violation in the K^0_S system means that the relation $A^{\overline{D}}_S(s_{-+}) = A^D_S(s_{+-})$ is not exactly true; and in addition, there is now a

dependence on $A_{\rm L}^{D}\ (s_{-+})$ which satisfies a different approximate symmetry, namely $A_{\rm L}^{\bar{D}}(s_{-+}) \simeq -A_{\rm L}^{D}(s_{+-})$. Grossman and Savastio describe these symmetry breaking effects in detail, but do not explicitly derive the corrections to the yield equations of Chapter 1, nor try to quantify the potential bias on γ in a measurement based on the binned yields. Instead, they derive expressions for the bias in a measurement obtained from phase-space integrated *CP* asymmetries. This is done for both GLW measurements that use $D \to K^0_{\rm S}X$ final states and for the $D \to K^0_{\rm S}h^+h^-$ final states; however, for their quantitative estimate of $\Delta\gamma$ the authors make an approximation that corresponds to assuming that the $D \to K^0_{\rm S}h^+h^-$ final state is a *CP* eigenstate, making the two results identical. The authors find that in this case, assuming a uniform experimental acceptance for all kaon decay times, the asymmetry has the form[1]

$$A = \frac{2r_B \sin\gamma \sin\delta_B + 2{\rm Re}[\epsilon]}{1 + r_B^2 - 2r_B\cos\gamma\cos\delta_B}, \tag{3.20}$$

If a measured value of A is interpreted to obtain γ without taking the ϵ term into account, it leads to a bias of

$$\Delta\gamma = -\frac{{\rm Re}[\epsilon]}{r_B\cos\gamma\sin\delta_B} + O(|\epsilon|). \tag{3.21}$$

The scaling $\Delta\gamma \sim \mathcal{O}(r_B/|\epsilon|)$ is the main result of the analysis by Grossman and Savastio. For $B^\pm \to DK^\pm$ decays, where $r_B^{DK^\pm} \simeq 0.1$ this suggests a bias at the percent level, which is negligible compared to current experimental uncertainties. However, in the $B^\pm \to D\pi^\pm$ case, where $r_B^{D\pi^\pm} \simeq 0.005$ [**?**], their result suggests relative biases that are potentially of $\mathcal{O}(1)$.

The conclusions are lacking on two accounts, however. Firstly, as made clear in Section 1.3.5, the $K^0_{\rm S}\pi^+\pi^-$ and $K^0_{\rm S}K^+K^-$ states are *far from CP* eigenstates. From the asymmetry expression in that section, it is clear that the bias in a determination of γ based on phase-space asymmetries will in fact scale as

$$\Delta\gamma \sim \mathcal{O}\left(\frac{|\epsilon|}{(2\mathcal{F}_+ - 1)r_B}\right), \tag{3.22}$$

which suggests that Grossman and Savastio severely *underestimates* the potential impact. This is described in detail in Section 3.2.3. More importantly, the analysis of the phase-space integrated asymmetry is in fact *irrelevant* to BPGGSZ measurements as they are currently performed: as described in Section 1.3.5 the information from

[1] In fact the expression in Eq. (3.20) is missing a term, as will be clear when an analogous expression is derived in detail in Section 3.2.3.

the global asymmetry is completely discarded. Therefore it is necessary to analyse the effects of kaon *CP*-violation on a full, binned analysis of $D \to K^0_S h^+ h^-$ decays, which is done in detail in the following sections. While the aim is to extend the analysis if Grossman and Savastio, the treatment in the following sections is completely independent of that in Ref. [**?**].

3.2 Impact on BPGGSZ measurements of γ: principles

The analysis of the impact on BPGGSZ measurements is carried out in two stages. This section treats the leading order effects analytically, and derives the overall order of magnitude of the expected bias in a general setting. Then Section 3.3 presents a detailed numerical study of the expected effect in measurements with the LHCb and Belle II experiments specifically, because these will be crucial to constrain γ during the coming decade [**?**, **?**].

3.2.1 Modified symmetry relations

In order to derive the corrections to the asymmetry relation $A^D_S(s_{-+}) \simeq A^{\overline{D}}_S(s_{+-})$, it it beneficial to express $A^D_{S(L)}$ in terms of the amplitudes

$$A^{(\overline{D})}_{1/2} = A(\,^{(}\overline{D}^{)0} \to K^0_{1/2}\pi^+\pi^-), \tag{3.23}$$

because these amplitude satisfy the exact symmetries $A^D_1(s_{-+}) = A^{\overline{D}}_1(s_{+-})$ and $A^D_2(s_{-+}) = -A^{\overline{D}}_2(s_{+-})$. This approach is different to that of Grossman and Savastio, but the final results are equivalent. After the decay of a D^0 meson to a neutral kaon, the kaon state is

$$\begin{aligned}\psi^0 &= A^D_1|K_1\rangle + A^D_2|K_2\rangle \\ &= N\left[(A^D_1 - \epsilon A^D_2)|K^0_S\rangle + (A^D_2 - \epsilon A^D_1)|K^0_L\rangle\right],\end{aligned} \tag{3.24}$$

with the normalisation constant $N = \sqrt{1+|\epsilon|^2}/(1-\epsilon^2)$. Thus it can be seen that

$$\begin{aligned}A^D_S(s_{+-}) &= N\left[(A^D_1(s_{+-}) - \epsilon A^D_2(s_{+-}))\right], \\ A^D_L(s_{+-}) &= N\left[(A^D_2(s_{+-}) - \epsilon A^D_1(s_{+-}))\right],\end{aligned} \tag{3.25}$$

with an analogous expression for the $\overline{D}^0$ decay amplitudes. Therefore, the generalised relations between the D^0 and $\overline{D}^0$ amplitudes are

$$\begin{aligned} A_{\rm S}^{\overline{D}}(s_{+-}) &= N[A_1^{\overline{D}}(s_{+-}) - \epsilon A_2^{\overline{D}}(s_{+-})] \\ &= N[A_1^{D}(s_{-+}) + \epsilon A_2^{D}(s_{-+})] = A_{\rm S}^{D}(s_{-+}) + 2N\epsilon A_2^{D}(s_{-+}), \\ A_{\rm L}^{\overline{D}}(s_{+-}) &= N[A_2^{\overline{D}}(s_{+-}) - \epsilon A_1^{\overline{D}}(s_{+-})] \\ &= -N[A_2^{D}(s_{-+}) + \epsilon A_1^{D}(s_{-+})] = -A_{\rm L}^{D}(s_{-+}) - 2N\epsilon A_1^{D}(s_{-+}). \end{aligned} \tag{3.26}$$

3.2.2 Relationship between the $K^0_{\rm S}$ and $K^0_{\rm L}$ amplitudes

The decay amplitude $A(D^0 \to K^0_{\rm S}\pi^+\pi^-)$ has been carefully studied, and a number of amplitude models have been published [**?**, **?**, **?**, **?**, **?**]. No models have been published for $D^0 \to K^0_{\rm L}\pi^+\pi^-$ decays. However, following an approach laid out by the CLEO collaboration [**?**], the two amplitudes can be related. Again, this is most easily done by relating the $A_1^D(s_{+-})$ and $A_2^D(s_{+-})$ amplitudes. In the isobar formalism, the decay amplitude $A(D^0 \to K_1\pi^+\pi^-)$ is expressed as a non-resonant constant amplitude plus a sum of resonances

$$A(D^0 \to K_1\pi^+\pi^-) = k_{NR} + \sum_{CF} k_i R^i(s_{K\pi^-}) + \sum_{DCS} k_j R^j(s_{K\pi^+}) + \sum_{R_{\pi\pi}} k_k R^k(s_{\pi^+\pi^-}). \tag{3.27}$$

The resonances are split into Cabibbo-favoured (CF) K^{*-} resonances, doubly Cabibbo-suppressed (DCS) K^{*+} resonances and $\pi\pi$ resonances.[2] The CF resonances couple to the $\overline{K}^0$ component of K_1 ($\propto K^0 + \overline{K}^0$), and therefore the corresponding k_i in the K_2 ($\propto K^0 - \overline{K}^0$) amplitude will have a relative minus sign. The DCS resonances couple to the K^0 component of K_1, and so the corresponding k_j in the K_2 amplitude will have a relative plus sign. For the h^+h^- resonances, there will be a coupling to both the K^0 and $\overline{K}^0$ components, however the coupling to the K^0 component is expected to be suppressed with a Cabibbo suppression factor $r_k e^{i\delta_k}$, where $r_k \simeq \tan^2\theta_C \simeq 0.05$ is determined by the Cabibbo angle θ_C and δ_k can take any value. Therefore, the k_k for these resonances have a relative $-(1 - 2r_k e^{i\delta_k})$ factor in the K_2 amplitude. The same effect leads to the differences in decay rates between $D^0 \to K^0_{\rm S}\pi^0$ and $D^0 \to K^0_{\rm L}\pi^0$ decays [**?**, **?**]. Thus, given a model of the

[2] In modern models, the $\pi\pi$ and $K\pi$ S-wave components are modelled via the K-matrix formalism and LASS parametrisations, respectively, instead of sums of individual resonances [**?**]. This does not alter the arguments below, as the R functions of Eq. (3.27) can equally well represent such terms.

form in Eq. (3.27), a model for the $A(D^0 \to K_2\pi^+\pi^-)$ amplitude will have the form

$$\begin{aligned} A(D^0 \to K_2\pi^+\pi^-) = k_{NR} + \sum_{CF}(-k_i)R^i(s_{K\pi^-}) + \sum_{DCS}(+k_j)R^j(s_{K\pi^+}) \\ + \sum_{R_{\pi\pi}}(-(1-2r_k e^{i\delta_k})k_k)R^k(s_{\pi^+\pi^-}). \end{aligned} \tag{3.28}$$

An important consequence of these substitution rules is that

$$A_2^D(s_{+-}) = -A_1^D(s_{+-}) + r_A \Delta A(s_{+-}), \tag{3.29}$$

where $r_A \simeq \tan^2\theta_C$ and $\Delta A(s_{+-}) \sim A_1^D(s_{+-})$ are of the same order of magnitude (at least when averaged over the bins used in γ measurements). This relation is sufficient to make the qualitative arguments of this section, while the full set of substitution rules above are used in the quantitative studies of Section 3.3.

3.2.3 Modification of the BPGGSZ yield equations

With suitable models to calculate $A_{\mathrm{S(L)}}^{(\overline{D})}$ (or $A_{1/2}^{(\overline{D})}$) and knowledge of $\Delta\chi$ for the materials relevant to an experimental setting, the relations derived in the preceding sections can be employed to calculate the expected phase-space bin yields, $N_i^{\pm}$, including the effects of kaon *CP* violation and material interaction. The decay rates have additional terms compared to those in Eq. (1.24), because the K_{L}^0 contribution must be taken into account

$$\mathrm{d}\Gamma(t, s_{-+}) \propto \left|\psi_{\mathrm{S}}(t, s_{-+}) + \epsilon\psi_{\mathrm{L}}(t, s_{-+})\right|^2, \tag{3.30}$$

where the time-dependence of $\psi_{\mathrm{S/L}}(t, s_{-+})$ is governed by Eq. (3.15), and the phase-space dependence is included in the state component, by defining $\psi_{\mathrm{S/L}}^0$ in terms of $A_{\mathrm{S(L)}}^{(\overline{D})}(s_{-+})$. For example, for the case of a $B^- \to DK^-$ decay, the definition is

$$\begin{aligned} \psi_{\mathrm{S/L}}^{0,B^-}(s_{-+}) &= A_{\mathrm{S}}^D(s_{-+}) + r_B e^{i(\delta_B-\gamma)} A_{\mathrm{S}}^{\overline{D}}(s_{-+}) \\ &= A_1^D(s_{-+}) - \epsilon A_2^D(s_{-+}) + r_B e^{i(\delta_B-\gamma)}\left(A_1^{\overline{D}}(s_{-+}) - \epsilon A_2^{\overline{D}}(s_{-+})\right) \\ &= A_1^D(s_{-+}) - \epsilon A_2^D(s_{-+}) + r_B e^{i(\delta_B-\gamma)}\left(A_1^D(s_{+-}) + \epsilon A_2^D(s_{+-})\right). \end{aligned} \tag{3.31}$$

It is useful to look at the corrections to the BPGGSZ yield expressions in Eq. (1.25) to lowest order in ϵ and $r_\chi = \frac{1}{2}\frac{\Delta\chi}{\Delta\lambda}$, the dimensionless parameter governing material interactions. For LHCb and Belle II the average $|r_\chi| \simeq 10^{-3}$, as detailed in the Section 3.3. To first order in r_χ, the time-dependent kaon states within a material, given in Eq. (3.15), simplify to [**?**]

$$\begin{aligned} \psi_{\mathrm{S}}(t, s_{+-}) &= e^{-\frac{i}{2}(\chi+\bar{\chi})t} e^{-i\lambda_{\mathrm{S}}t}\left(\psi_{\mathrm{S}}^0(s_{+-}) - r_\chi\left(1 - e^{-i\Delta\lambda t}\right)\psi_{\mathrm{L}}^0(s_{+-})\right), \\ \psi_{\mathrm{L}}(t, s_{+-}) &= e^{-\frac{i}{2}(\chi+\bar{\chi})t} e^{-i\lambda_{\mathrm{L}}t}\left(\psi_{\mathrm{L}}^0(s_{+-}) + r_\chi\left(1 - e^{+i\Delta\lambda t}\right)\psi_{\mathrm{S}}^0(s_{+-})\right). \end{aligned} \tag{3.32}$$

By inserting these expressions into Eq. (3.30) and employing the definition in Eq. (3.31) (and a similar definition for B^+ decays), the binned yields can be calculated by an integration over time and phase space. In the remainder of this section, it is assumed that the experimental time acceptance is $\eta(t) = 1$ for all times and that r_χ is constant at all times; more realistic assumptions are introduced in Section 3.3. In this case, the binned yields are given by the expression

$$\begin{aligned} N_i^- &= h_B^{-'}\left(\hat{K}_{+i} + r_B^2\hat{K}_{-i} + 2\sqrt{\hat{K}_{+i}\hat{K}_{-i}}(x_-\hat{c}_i + y_-\hat{s}_i) + O(r\epsilon)\right), \\ N_i^+ &= h_B^{+'}\left(\hat{K}_{-i} + r_B^2\hat{K}_{+i} + 2\sqrt{\hat{K}_{+i}\hat{K}_{-i}}(x_+\hat{c}_i - y_+\hat{s}_i) + O(r\epsilon)\right), \end{aligned} \tag{3.33}$$

where a number of new parameters have been defined, and where $O(r\epsilon)$ denotes terms of $O(r_A\epsilon)$, $O(r_B\epsilon)$, $O(r_A r_\chi)$, and $O(r_B r_\chi)$. Since $r_B \sim r_A \sim 10^{-1}$ (in $B^\pm \to DK^\pm$ decays) and $r_\chi \sim \epsilon \sim 10^{-3}$, these terms are all of the same order of magnitude.

The new normalisation constants $h_B^{\pm'} = h_B^\pm(1 + |\epsilon + r_\chi|^2\frac{\Gamma_S}{\Gamma_L} \mp \Delta h)$ are defined in terms of

$$\Delta h = 2\mathrm{Re}[\epsilon + r_\chi] - 4\frac{\Gamma_S}{\Gamma_L + \Gamma_S}\frac{\mathrm{Re}[\epsilon + r_\chi] + \mu\mathrm{Im}[\epsilon + r_\chi]}{1 + \mu^2}, \quad \mu = 2\frac{m_L - m_S}{\Gamma_L + \Gamma_S}. \tag{3.34}$$

The $\hat{K}_i$ parameters are defined to be

$$\hat{K}_i = \frac{1}{1 + |\epsilon + r_\chi|^2\frac{\Gamma_S}{\Gamma_L}}\left(K_i^{(1)} + |\epsilon + r_\chi|^2\frac{\Gamma_S}{\Gamma_L}K_i^{(2)}\right), \tag{3.35}$$

in which the $K_i^{(1/2)}$ parameters are phase-space integrals, defined as in Eq. (1.27) but for $A_{1/2}^D$. To lowest order, the $\hat{K}_i$ correspond to the fractional D^0 decay yield in each bin, as obtained in a measurement that averages D^0 and $\overline{D}^0$ decays, and assumes the $A_S^{\overline{D}}(s_{-+}) = A_S^D(s_{+-})$ symmetry to be exact:

$$K_i^{\mathrm{meas}} \equiv \frac{N_i^D + N_{-i}^{\overline{D}}}{\sum_j N_j^D + N_{-j}^{\overline{D}}} = \hat{K}_i + \mathcal{O}(r\epsilon). \tag{3.36}$$

Here, N_i^D ($N_i^{\overline{D}}$) is the expected yield of flavour tagged D^0 ($\overline{D}^0$) mesons into bin i of the D decay phase-space.

In similar fashion, the parameters $(\hat{c}_i, \hat{s}_i)$ have been introduced to denote the *measured* average strong-phases, which are expected to differ from (c_i, s_i) at $O(\epsilon)$, since neutral kaon *CP* violation is not taken into account in the measurements by CLEO. Thus, any corrections arising if $\hat{c}_i, \hat{s}_i)$ and (c_i, s_i) are substituted in Eq. (3.33) will appear in the $O(r_B\epsilon)$ terms.

Two observations can be made from the expression in (3.33). The first is that the phase-space *distribution* is only changed at $O(r\epsilon)$ compared to the expression in

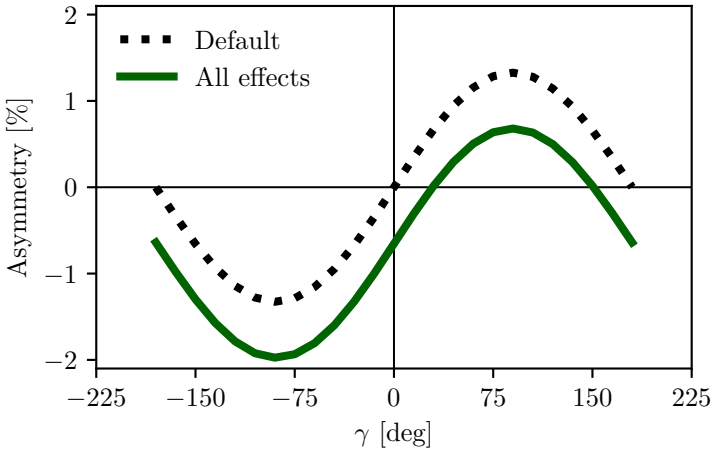

Figure 3.1: The asymmetry A_{total} as a function of γ calculated to $O(\epsilon)$ using Eq. (3.37). The calculation is made using for (black dotted line) the default case where $\Delta h = 0$ and (green) including neutral kaon *CP*-violation and material interaction with $r_\chi = \epsilon$.

Eq. (1.25), if the measured $\hat{K}_i$ are used in the experimental analysis. This equally true whether the K_i are fitted in the signal channel along with $x_\pm$ and $y_\pm$, as is the case in the measurement presented in the thesis, or if they are obtained in a control channel with flavour tagged D decays, according to Eq. (3.36). As the $D^0 - \overline{D}^0$ interference term that provides sensitivity to γ enters at order $O(r_B)$, the impact on γ measurements can be expected to be $\Delta\gamma/\gamma \sim O(r\epsilon/r_B)$. For $B \to DK$ analyses, where $r_B \simeq 0.1$, this is at the permille level, so the induced $\Delta\gamma$ bias can be expected to be smaller than 1°. Even in the case of $B^\pm \to D\pi^\pm$ decays, this suggests biases that are maximally a few percent. This is the main result of the chapter, because it means that the effect of neutral kaon *CP* violation and material interaction is small compared to the precision of the measurement that is the main subject of the thesis.

The second observation relates to potential future measurements of γ, which may also include sensitivity from the total, phase-space-integrated yield asymmetry

$$A_{\text{total}} = \frac{N^- - N^+}{N^- + N^+} = \frac{2(2\mathcal{F}_+ - 1)r_B \sin\delta_B \sin\gamma + \Delta h}{1 + r_B^2 + 2(2\mathcal{F}_+ - 1)r_B \cos\delta_B \cos\gamma} + O(r\epsilon), \tag{3.37}$$

where the definition of $\mathcal{F}_+$ from Section 1.3.5 has been employed. In the limit $r_B \to 0$ the expression agrees with the result for the analogous asymmetry in $D^\pm \to \pi^\pm K^0_S$ decays in Ref. [**?**], evaluated to $O(\epsilon)$ for an infinite and uniform time-acceptance. As hinted at above, the fact that $\mathcal{F}_+ \simeq 0.5$ means that the asymmetry due to γ being non-zero is not $\mathcal{O}(r_B)$, but of approximately the same order of magnitude as the asymmetry due to *CP* violation in the neutral kaon sector, governed by Δh. This is illustrated in Fig. 3.1, where the expression in Eq. (3.37) is plotted in the default

case where $\Delta h = 0$, using the model in Ref. [?] to calculate K_i and c_i, as well as including neutral kaon *CP* violation and material interaction effects, calculated using $r_\chi = \epsilon$, with ϵ taking the value in Eq. (3.12). The asymmetry changes significantly when including the latter effects. Therefore, measurements based only on the global asymmetry will suffer relative biases of tens of degrees, not a few degrees, if neutral kaon *CP* violation and material interaction is not taken into account.

3.3 Impact on BPGGSZ measurements of γ: LHCb and Belle II measurements

The previous section has established that the bias due to neutral kaon *CP* violation and material interaction is at the sub-percent level for measurements based on $B^\pm \to DK^\pm$ decays, and just a few percent in $B^\pm \to D\pi^\pm$ decays. Thus, the effects only contribute a manageable systematic uncertainty in the measurement that is the subject of the thesis. However, the expected precision on γ measurements will increase significantly in the coming decade, as both the LHCb [?] and Belle II [?] collaborations expect to make BPGGSZ measurements that measure γ with a precision of 1–3°. Therefore a deeper understanding of the expected bias for these specific experiments is important.

This section details a study, where the equations of the previous section are evaluated numerically to all orders, and care is taken to realistically model the experiment specific conditions. The scope of the original analysis, published in Ref. [?], was a stand-alone paper that covers both LHCb and Belle II, and which therefore does not rely on full detector simulation. Instead the following approaches are taken to model the necessary input

- the experimental time-acceptance is modelled based on the detector geometry and typical neutral kaon momentum spectrum
- the material interaction is included, using the material budget information available in the technical design reports on each experiment
- both the time-acceptance and material interaction depends on the neutral kaon momentum, for which realistic distributions are estimated using the `RapidSim` simulation package [?].

Each input is described in detail in the following sections. The study has been repeated to assign a systematic uncertainty to the LHCb measurement in Chapter 4, with slight adjustments to match the exact fit setup and with the inputs above extracted from full LHCb simulation. This is described further in Section 3.3.7.

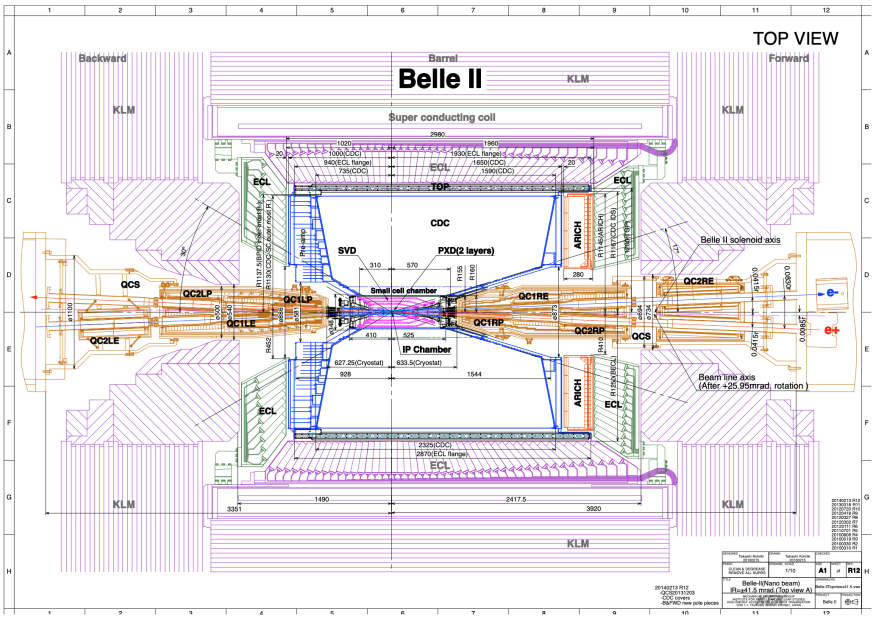

Figure 3.2: Schematic of the Belle II detector, reproduced from Ref. [**?**].

3.3.1 Detector geometries

The LHCb geometry and sub detectors are described in details in Chapter 2. In the LHCb measurement discussed in Chapter 4, the K^0_S mesons are reconstructed in the $\pi^+\pi^-$ final state and two distinct categories of decay are considered, depending on where in the detector the K^0_S decay occurs. The categories have very different decay-time acceptance, and therefore two scenarios are considered for LHCb: one in which the decay products of the K^0_S leave reconstructed tracks in both the silicon vertex detector and downstream tracking detectors (denoted *long-long* or LL), and one in which the decay products of the K^0_S only leave tracks in the downstream tracking detectors (denoted *down-down* or DD).

The Belle II detector is a general purpose spectrometer, built to to collect data from asymmetric e^+e^- collisions made by the SuperKEKB accelerator in Japan []. A schematic of the detector is shown in Fig. 3.2. The relevant sub detectors for the present study are the tracking detectors: a central silicon vertex detector, comprised of a total of six layers within 140 mm of the beam, and a large volume drift chamber with 56 wire layers, extending to a radius of 1130 mm [**?**]. A single scenario is considered for Belle II, because essentially all the K^0_S mesons produced in signal decays in Belle II decay within the tracking volume, with more than 90 % decaying in the vertex detector according to the studies described below. Thus, three scenarios are considered in total: LL LHCb, DD LHCb, and Belle II.

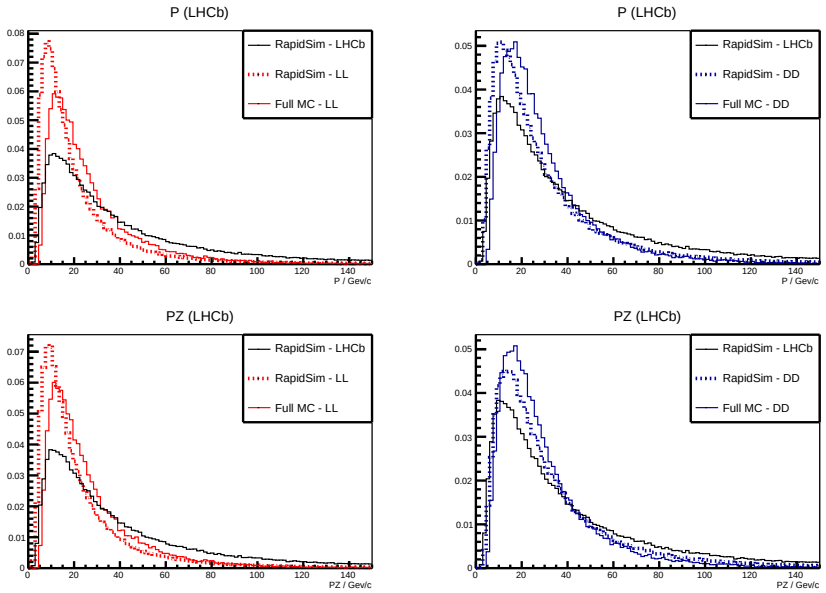

Figure 3.3: Momentum spectra for the K^0_S meson in LHCb, as generated using `RapidSim` (black lines) directly, as well as reweighed to match decay time acceptance in the (red) LL and (blue) DD data categories of LHCb. The LHCb spectra are compared with the spectra in fully simulated signal decays, for both (dotted red lines) LL and (dotted blue lines) DD data categories.

3.3.2 Kaon momentum distributions

The neutral kaon momentum distributions are obtained using `RapidSim` [?], a simple tool to generate MC samples. `RapidSim` has an inbuilt capability to generate decays of B mesons with the kinematic distribution found in LHCb collisions and falling in the LHCb acceptance. However, the distributions need to be reweighted to take the kaon-decay-time acceptance into account. After being reweighted, the `RapidSim` momentum spectra are reasonably close to those found in full LHCb simulation samples of $B^\pm \to D(\to K^0_S\pi^+\pi^-)K^\pm$ decays, as seen in Fig. 3.3

At Belle II, the signal B mesons stem from decays of $\Upsilon(4S)$ mesons produced in asymmetric electron-positron collisions. This leads to substantially different decay kinematics in comparison to those found at LHCb. The momentum distribution in Belle II is estimated by letting `RapidSim` decay B mesons with a momentum of 1.50 GeV/c along the z-axis using `RapidSim`, corresponding to the $\gamma\beta = 0.28$ boost of the centre-of-mass system in Belle II when operated at the $\Upsilon(4S)$ resonance [?]. A perfect 4π angular acceptance is assumed. It is not necessary to reweigh the Belle II momentum spectrum to account for the kaon-decay-time acceptance because all produced K^0_S mesons decay in the tracking volume.

The resulting momentum distributions for the three types of sample are shown in Fig. 3.4.

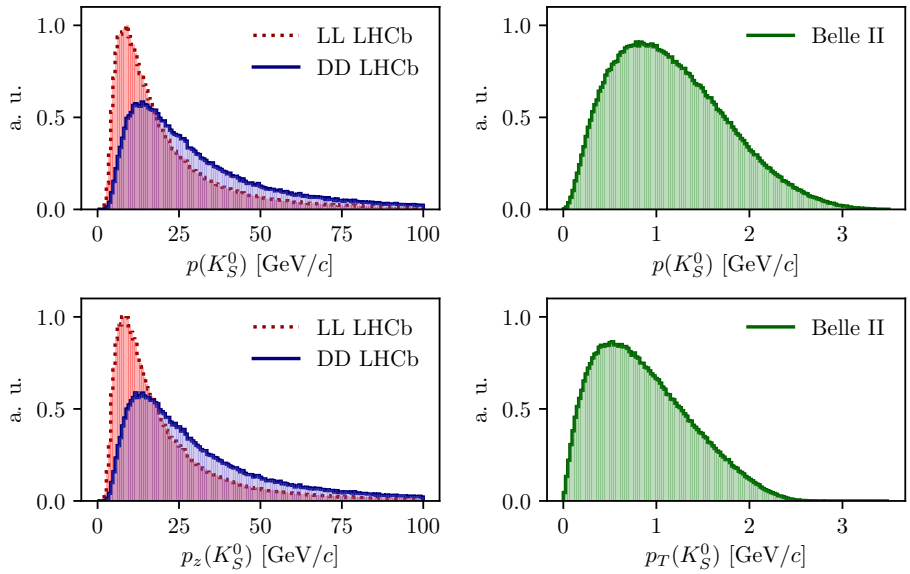

Figure 3.4: Momentum distributions for the LHCb (red dotted line) LL and (blue) DD categories, as well as (green) Belle II, obtained using `RapidSim`.

3.3.3 Experimental time acceptance

In order to model the experimental time acceptance, the time-dependent decay rates are only integrated over a finite time interval (τ_1, τ_2). The intervals are defined for each of the three experimental categories, by requiring that a neutral kaon, if produced at $x = y = z = 0$ with momentum $p = (p_T, p_z)$, decays within the relevant part of the corresponding detector. For the LL LHCb category, it is required that the kaon decays before reaching $z_{max} = 280\,\text{mm}$, corresponding to a decay where the decay products traverse at least 3 VELO segments (ignoring a number of widely spaced VELO segments placed at a distance of up to $z = 750\,\text{mm}$ from the interaction point) [?]. For the DD LHCb category a decay at $z \in [280, 2350]\,\text{mm}$ is required, corresponding to decay between the LL cut-off and the first downstream tracking station [?]. The time acceptance has a significant impact for the LHCb categories, where some 20 % of the kaons escape the tracking stations completely before decaying.

For Belle II, it is assumed that the K^0_S reconstruction is similar to the Belle K^0_S reconstruction, which is based on a neural network and reconstructs K^0_S decays for which the decay product leave tracks in both the drift chamber and silicon vertex detectors, as well as decays that leave tracks in the drift chamber only [?, ?]. Therefore, the K^0_S decay is required to be within $r_{max} = 1130\,\text{mm}$ of the beam axis, corresponding to a decay within the outer radius of the drift-chamber. In practice,

most of the kaons decay inside the silicon vertex detector, and requiring a decay before 1130 mm is essentially equivalent to having no time cut-off.

3.3.4 Detector material budget

The effect of the material interaction is governed by parameter $\Delta\chi$ of Eq. (3.16). The parameter varies along a given kaon path, as the kaon intersects detector components made of different materials. In these studies, the calculations are simplified by using a single average material parameter for each experimental scenario. The average material parameters can be estimated for a given experimental scenario by considering the type and length of material traversed by a kaon in the relevant sub-detector(s). The average value is estimated, by exploiting that $\Delta\chi$ is related to the forward scattering amplitude f ($\bar{f}$) of K^0 ($\overline{K}^0$) mesons in a given material [**?**, **?**]

$$\Delta\chi = -\frac{2\pi\mathcal{N}}{m_K}(f - \bar{f}) = -\frac{2\pi(N_A\rho/A)}{m_K}(f - \bar{f}), \tag{3.38}$$

where $\mathcal{N} = N_A\rho/A$ is the scattering centre density of the material, m_K is the mass of the kaon state, A and ρ are the nucleon number and density of the material, and N_A is Avogadro's number. Measurements made for a range of nuclei [**?**] show that in the momentum range $p_K \in [20, 140]\,\mathrm{GeV}/c$

$$\left|\frac{f - \bar{f}}{p_K}\right| = 2.23\frac{A^{0.758}}{p_K^{0.614}(\,\mathrm{GeV}/c)}\ \mathrm{mb}, \quad \arg[f - \bar{f}] = -\frac{\pi}{2}\,(2 - 0.614)\,, \tag{3.39}$$

where the phase of Δf is determined via a phase-power relation [**?**]. In the numerical studies presented here, Eq. (3.39) is also used for the low momentum neutral kaons in the Belle II calculations, as a more detailed modelling of the low momentum $\Delta\chi$ based on Ref. [**?**] is found to yield very similar results. The scattering centre density $\mathcal{N}$ is approximated as being constant, equal to the average density along a neutral kaon path due to its intersection with different detector segments. This average is estimated using the simplifying assumption that the total detector material budget is due to silicon. In practice, $\mathcal{N} = N_A\rho/A$ is calculated using $A = 28$ and $\rho = f^{\mathrm{Si}}\rho^{\mathrm{Si}}$, where $f^{\mathrm{Si}} < 1$ is the average fraction of a neutral kaon path length that is inside detector material, estimated via the known dimensions of the detector, the average nuclear interaction length seen by a track traversing it cf. the technical design reports [**?**, **?**], and the nuclear interaction length of silicon $\lambda_I^{\mathrm{Si}} = 465.2\,\mathrm{mm}$ [**?**]. The average value of $r_\chi = \frac{1}{2}\frac{\Delta\chi}{\Delta\lambda}$, which governs the size of the matter regeneration effect, can be calculated for the three considered experimental scenarios and satisfy $|r_\chi^{\mathrm{LL}}| = 2.7 \times 10^{-3}$, $|r_\chi^{\mathrm{DD}}| = 2.2 \times 10^{-3}$, and $|r_\chi^{\text{Belle II}}| = 1.0 \times 10^{-3}$.

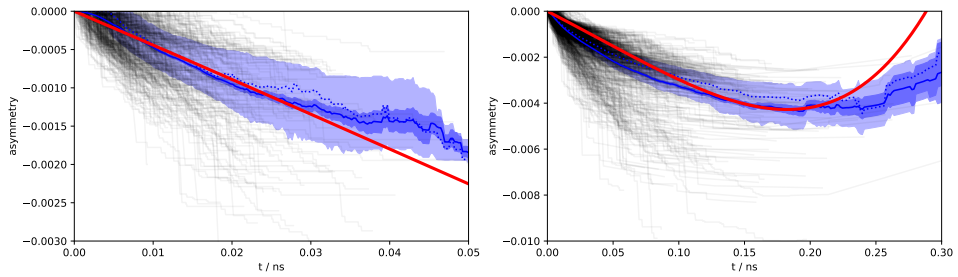

Figure 3.5: The asymmetry in Eq. (3.40) as a function of time for (left) LL and (right) DD K^0_S tracks in a simulated LHCb sample. The black lines show individual tracks. The light blue area is the central 50 % quantile, the dark blue area is the 1σ uncertainty band on the mean. The red lines are calculated using the average $\Delta\chi$ values that are also used in the calculation of biases in BPGGSZ measurements.

The neutral kaon tracks in LHCb generally pass through somewhere between zero (for a significant amount of the LL tracks) and a hundred (for some DD tracks) distinct detector segments. Therefore it is worth examining the degree to which using a single average $\Delta\chi$ value, obtained following the procedure outlined above, provides a reasonable description of the average material interaction. This can be done using full LHCb simulation, where the kaon state for a simulated track can be evaluated at all times, by applying Eq. (3.15) iteratively for each detector segment the track traverses, using a $\Delta\chi$ value appropriate for that segment. This is done in Fig. 3.5 for a simple observable: the yield asymmetry

$$A_{K^0} = \frac{|\psi_{K^0}(t)|^2 - |\psi_{\overline{K}^0}(t)|^2}{|\psi_{K^0}(t)|^2 + |\psi_{\overline{K}^0}(t)|^2}, \tag{3.40}$$

where $\psi_{K^0}(t)$ ($\psi_{\overline{K}^0}(t)$) is the amplitude for an initial K^0 ($\overline{K}^0$) to decay to two pions at time t. In this calculation, it is assumed that $\epsilon = 0$ to isolate the material effect with no asymmetry contribution from the inherent *CP*-violation in the neutral kaon sector. While the track-by-track asymmetries are found to differ significantly depending on the exact detector segments a track intersects, the average asymmetry is seen to evolve smoothly as a function of decay time, and in reasonable agreement with the asymmetry value that is calculated using the average $\Delta\chi$ values estimated above.

The LHCb detector is undergoing a significant upgrade prior to the start of the LHC Run 3. However, the material budget and geometry of the relevant sub-detectors will be similar to the sub-detectors used during Run 1 and 2 [**?**, **?**]. Hence the results of this study will be valid for measurements during the upgrade phases of LHCb, even though the detector parameters presented in this section relate to the original LHCb detector.

3.3.5 Calculation procedure

The main idea in the bias study is to calculate the BPGGSZ bin yields including the full effect of neutral kaon *CP* violation and material, fit them using the default equations of Chapter 1, and obtain the bias $\Delta\gamma = \gamma - \gamma^0$ due to the kaon effects not being considered in the parameter extraction. For the purpose of Ref. [**?**], a simple fit setup of a single $B^\pm \to Dh^\pm$ mode is investigated, where the K_i parameters are determined in a control channel with the relevant experimental acceptance. This setup is modified in the study used to assign a systematic uncertainty on the LHCb measurement of Chapter 4, as described in Section 3.3.7 below.

In practice, the amplitude model for $D^0 \to K^0_S\pi^+\pi^-$ decays in Ref. [**?**] is taken to represent the $A_1(s_{+-})$ amplitude. Then $A_2(s_{+-})$ is obtained as described in Section 3.2.2. In terms of A_1 and A_2, the amplitudes $A^{(\overline{D})}_{S(L)}(s_{+-})$ can be expressed and related via Eqs. (3.25) and (3.26), and the full signal decay amplitudes as a function of phase-space coordinates, time, and the material interaction parameter $\Delta\chi$ can be calculated for a given set of input parameters $(\gamma^0, r^0_B, \delta^0_B)$. The squared decay amplitudes are then integrated over phase space and the kaon decay times to obtained the binned signal yield.

The signal yields depend on the momentum via the time-acceptance parameters τ_1 and τ_2, and because the material interaction parameter $\Delta\chi$ is momentum dependent. Therefore, the yields are averaged over the K^0_S momentum distributions of LHCb and Belle II.

The parameters $x_\pm$ and $y_\pm$ are determined by a maximum likelihood fit to the calculated yields, after which the fit result and covariance matrix are interpreted in terms of the physics parameters (γ, r_B, δ_B) using another maximum likelihood fit [**?**]. In the fits, the K_i are obtained using the definition $K_i = K_i^{\text{meas}} = (N_i^D + N_{-i}^{\overline{D}})/(\sum_j N_j^D + N_{-j}^{\overline{D}})$, in terms of the expected yields N_i^D ($N_i^{\overline{D}}$) of a flavour-tagged D^0 ($\overline{D}^0$) decays in bin i of the D decay phase space, calculated as described above for $r^0_B = 0$. This corresponds to experimentally measuring the K_i in a control channel, and takes the effect of neutral kaon *CP* violation and material interaction on K_i measurements into account, as well the experimental time acceptance. The (c_i, s_i) are calculated using $A_1(s_{+-})$ and the experimental time acceptance is taken into account in this calculation as well.

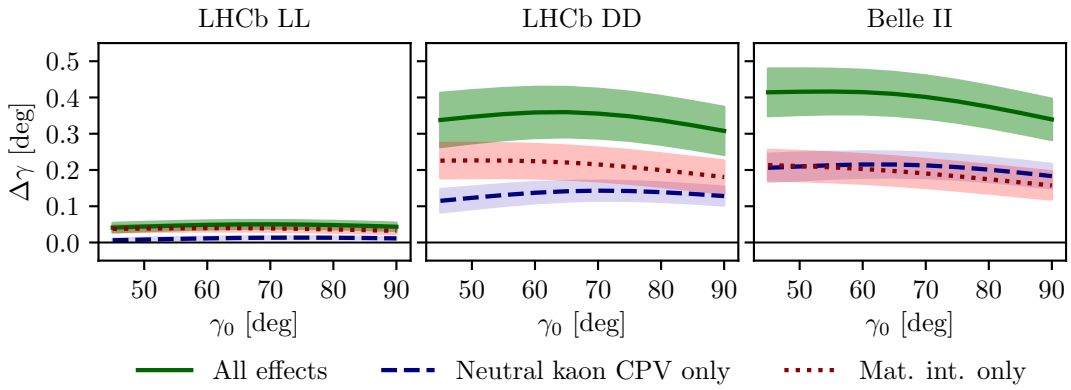

Figure 3.6: The bias $\Delta\gamma$ as a function of input γ_0 for (left) the LL LHCb category, (centre) the DD LHCb category, and (right) Belle II. The bias is calculated due to (blue, dashed line) neutral kaon *CP* violation alone, (red, dotted line) material interaction alone, and (green line) both effects. The shaded region shows the estimated 1σ uncertainty band.

3.3.6 Results

The obtained bias $\Delta\gamma$ is shown as a function of input γ^0 for the various experimental conditions in Fig. 3.6. The calculations are made using $(r_B^0, \delta_B^0) = (0.1, 130^\circ)$, approximately equal to the physics parameters relevant for $B^\pm \to DK^\pm$ decays [**?**,**?**]. The bias does not vary significantly with γ^0 in the plotted range, which includes the world average value of direct γ measurements as well as the values obtained in full unitarity-triangle fits [**?**,**?**,**?**], and for all cases, the bias is found to be below 0.5°, corresponding to relative biases of about half a percent. Thus the biases are of $O(r\epsilon/r_B)$ as expected, given the arguments of Section 3.2.3. The contributions from the individual K^0_S CPV and material interaction effects are also shown. It is seen that the neutral kaon *CP* violation and material interaction effects leads to approximately equal biases in all three cases.

Given the decay-time acceptance and momentum distribution for each experimental category, the mean life time, $\langle\tau\rangle$, of the reconstructed kaons can be calculated. In terms of the K^0_S lifetime $\tau_{K^0_S} = (0.895 \pm 0.004) \times 10^{-11}\,\text{s}$ [**?**], $\langle\tau_{\text{LL}}\rangle \simeq 0.1\tau_{K^0_S}$ for the LHCb LL category, $\langle\tau_{\text{DD}}\rangle \simeq 0.8\tau_{K^0_S}$ for the LHCb DD category, and at Belle II $\langle\tau_{\text{Belle II}}\rangle \simeq \tau_{K^0_S}$. The difference in average kaon lifetime is reflected in the observed biases, which are found to be larger in the samples with longer lived kaons. The very small effect in the LL category is to be expected because the *CP*-violation effect due to K^0_S not being *CP*-even is approximately cancelled by the *CP*-violation effect arising from $K^0_S - K^0_L$ interference for kaons with decay times much smaller than $\tau_{K^0_S}$ [**?**].

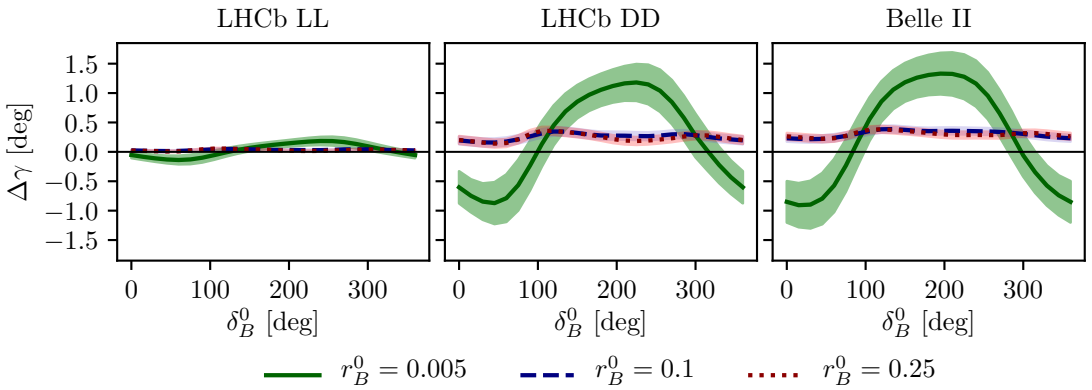

Figure 3.7: The bias $\Delta\gamma$ as a function of input δ_B for (left) the LL LHCb category, (centre) the DD LHCb category, and (right) Belle II. The bias is calculated for $\gamma = 75^\circ$ and (green line) $r_B = 0.005$, (blue, dashed line) $r_B = 0.1$, and (red, dotted line) $r_B = 0.25$. The shaded region shows the estimated 1σ uncertainty band.

The uncertainty bands in Fig. 3.6 are calculated by repeating the study while varying some of the inputs. The model dependence of the predicted biases is probed by repeating the study using two other amplitude models as input for $A_1(s_{+-})$ and $A_2(s_{+-})$: the model published in Ref. [**?**] and the model included in EvtGen [**?**]. hen defining $A_2(s_{+-})$ in terms of $A_1(s_{+-})$, there is an uncertainty due to the unknown (r_k, δ_k) parameters used to describe the $\pi\pi$ resonance terms. This uncertainty is assessed by making the study with several different random realisations of the parameter set. The studies are repeated while varying the time acceptances and material densities with $\pm 10\,\%$. There is an additional uncertainty due to the use of simulation samples generated with `RapidSim` to describe the kaon momentum distribution, in lieu of full detector simulations.

There is also an uncertainty from the use of (c_i, s_i) as calculated using $A_1(s_{+-})$. It is to be expected that the measured values $(\hat{c}_i, \hat{s}_i)$ from the CLEO collaboration differ by those calculated using $A_1^D(s_-, s_+)$ by terms of $O(\epsilon)$ due to neutral kaon *CP* violation, which is not taken into account in the measurement [**?**]. These corrections can be calculated via a procedure analogous to the one used to estimate the corrections on measurements of γ in this paper. However, as these corrections are much smaller than the experimental uncertainties in the measurement, they have not been studied further.

For the purpose of this thesis, it is important to consider the bias in measurements that use $B^\pm \to D\pi^\pm$ decays as well, and other B decay modes can also be used in BPGGSZ measurements, such as $B^\pm \to D^*K^\pm$, $B^\pm \to DK^{*\pm}$, and $B^0 \to DK^{*0}$. For the purpose of the study presented here, the main difference between the decay

channels is that they have different values of r_B and δ_B. Figure 3.7 shows $\Delta\gamma$ as a function of input δ_B^0, for $\gamma^0 = 75^\circ$ and three different values of r_B^0. Aside from $r_B^0 = 0.1$, the results are shown for $r_B^0 = 0.005$, which corresponds to the expectation in $B^\pm \to D\pi^\pm$ decays [**?**] and $r_B^0 = 0.25$, which corresponds to $B^0 \to DK^{*0}$ decays [**?**, **?**]. The most notable feature is that the biases are significantly larger in the $B^\pm \to D\pi^\pm$ case. This is expected: the r_B^0 dependent behaviour is governed by the relative importance of different $O(r\epsilon)$ correction terms to the phase-space distribution. There are terms of both $O(r_A\epsilon)$ and $O(r_B\epsilon)$[3], which lead to expected biases of size $O(r_A\epsilon/r_B)$ and $O(r_B\epsilon/r_B) = O(\epsilon)$, respectively, cf. the discussion of Section 3.2.3. In the $B^\pm \to D\pi^\pm$ case, the $O(r_A\epsilon)$ correction terms dominate because $r_A/r_B \simeq (0.05/0.005) = 10$. This explains the relatively large bias, as $|r_A\epsilon/r_B^{D\pi}| \simeq 4\%$. The bias is seen to be up to $\pm 1.5^\circ$, but only about $+0.2^\circ$ with the expected value of $\delta_B^{D\pi} \simeq 300^\circ$ [**?**, **?**]. These biases are *much smaller* than the precision on γ that is obtainable in a $B^\pm \to D\pi^\pm$ analysis with current experimental yields, and do thus not pose a problem. In the $r_B^0 = 0.1$ and $r_B^0 = 0.25$ cases the $O(r_B\epsilon)$ correction terms dominate, and the biases are of $O(\epsilon)$, independent of the r_B^0 value. Therefore both cases have biases of similar size.

Further, it is clear that the biases depend on δ_B^0 and that the oscillation period of the δ_B dependence is different between the $r_B^0 = 0.005$ case and the $r_B^0 \in \{0.1, 0.25\}$ cases. It is to be expected that $\Delta\gamma$ oscillates as a function of δ_B^0, because δ_B^0 enters the yield equations via $\cos(\delta_B^0 \pm \gamma)$ and $\sin(\delta_B^0 \pm \gamma)$ terms. As explained above, the $O(r_A\epsilon)$ terms dominate the $B^\pm \to D\pi^\pm$ bias, and these are independent of δ_B^0. The $O(r_B\epsilon)$ terms, however, are important for the bias corrections for larger r_B values, and the terms include factors of $\cos(\delta_B^0 \pm \gamma)$ and $\sin(\delta_B^0 \pm \gamma)$. This explains the different bias dependence on δ_B^0.

While the input value of $\gamma^0 = 75^\circ$ was chosen for these studies, there is minimal variation in the results if another value of γ^0 in the range $[60^\circ, 85^\circ]$ is used.

3.3.7 Coupled $B^\pm \to DK^\pm$ and $B^\pm \to D\pi^\pm$ measurements

The studies presented above have been extended on two accounts in order to assign a systematic uncertainty to the LHCb measurement presented in Chapter 4. Firstly, full LHCb simulation has been used to obtain the momentum distributions, as well as to fit a better description of the time acceptance and the reconstruction efficiency profile over the D-decay phase space. Secondly, the fit setup is modified

[3]There are similar terms of $O(r_A r_\chi)$ and $O(r_B r_\chi)$, but as ϵ and r_χ are of the same order of magnitude, these terms can be treated completely analogously to the $O(r_A\epsilon)$ and $O(r_B\epsilon)$ terms, and have been left out of the discussion for brevity.

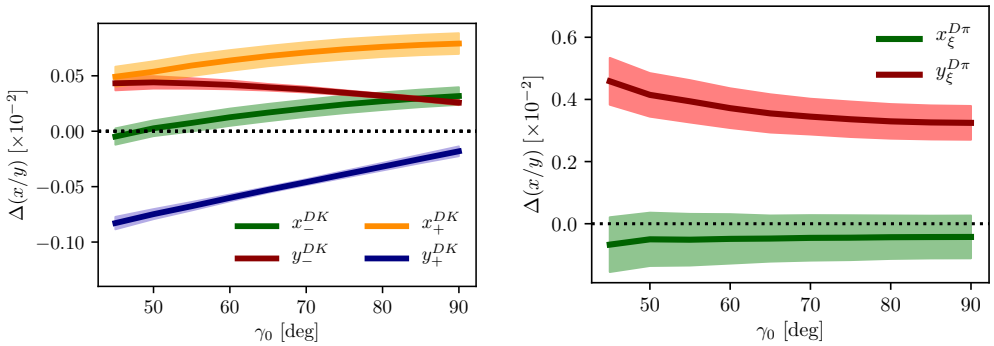

Figure 3.8: The bias on (left) the $B^\pm \to DK^\pm$ and (right) $B^\pm \to D\pi^\pm$ *CP*-violation observables in the LHCb DD category, evaluated in bias studies with inputs based on full LHCb simulation, calculated as a function of input γ_0.

to correspond to the experimental approach described in Section 1.4 and Chapter 4: the signal yields are calculated for both the $B^\pm \to DK^\pm$ and $B^\pm \to D\pi^\pm$ channels, and fitted in a combined fit to obtain $(x_\pm^{DK}, y_\pm^{DK}, x_\xi^{D\pi}, y_\xi^{D\pi})$, where the F_i parameters are allowed to float in the fit. The biases obtained for each observable are shown in Fig. 3.8, evaluated using the time-acceptance, momentum distribution, and material budget relevant for the DD category (since the effect in the LL category is much smaller). As will be clear in Chapter 4, these biases are all significantly smaller than the corresponding statistical uncertainties. Thus, the effects of neutral kaon *CP* violation and material interactions contribute a manageable systematic uncertainty in current BPGGSZ measurements, even if the $B^\pm \to D\pi^\pm$ channel is promoted to a signal channel.

As the statistical uncertainty becomes comparable with the bias effects described in this chapter, the systematic uncertainty should be assigned by a more accurate study, incorporating the traversed material on a track-by-track basis in full detector simulation. Such a detailed calculations can also be used to apply a bias correction if desired.

3.4 Concluding remarks

The analysis presented in this chapter has shown the expected impact of neutral kaon *CP* violation and material interaction on current BPGGSZ measurements to be small compared to the statistical uncertainties; first by simple order-of-magnitude estimates and then by a detailed calculation of the expected effect in LHCb and Belle II.

While the calculations were made for the case of $D \to K^0_S\pi^+\pi^-$ decays, the BPGGSZ approach can of course also be applied in other D-decay final states,

such as $D \to K^0_S K^+ K^-$ and $D \to K^0_S \pi^+ \pi^- \pi^0$. The biases on measurements of γ based the D decay phase-space distributions should be of similar size in these decay channels. The impact on γ measurements based on the phase-space-integrated yield asymmetry can be expected to be tens of degrees for the $D \to K^0_S K^+ K^-$ channel, where the yield asymmetry is expected to be around 2 %, for the reasons explained in Section 3.2.3. The $D \to K^0_S \pi^+ \pi^- \pi^0$ decay, however, is dominantly *CP*-odd [**?**], and the bias in measurements based on the total asymmetry is therefore expected to be $O(\epsilon/r_B)$, ie. a few degrees [**?**]. More precise calculations of the biases would require a repeat of the study included here, with relevant amplitude models and binning schemes in place.

The chapter focuses on the model-independent, binned approach that is the subject of the thesis. However, the underlying mechanism that determines the scale of the bias, namely that the phase-space *distribution* of signal decays is unaffected at $\mathcal{O}(\epsilon)$ and $\mathcal{O}(r_\chi)$, is independent on the exact measurement approach. Therefore it is expected that amplitude-model-based measurements and measurements made with new unbinned methods such as those in Ref [**?**] will be similarly biased if kaon *CP* violation and regeneration are not accounted for.

4

A GGSZ measurement with $B^{\pm} \to Dh^{\pm}$ decays

This chapter describes a model-independent BPGGSZ measurement of γ with $B^{\pm} \to DK^{\pm}$ and $B^{\pm} \to D\pi^{\pm}$ decays where $D \to K^0_S\pi^+\pi^-$ and $D \to K^0_S K^+K^-$, commonly denoted $B^{\pm} \to D(\to K^0_S h^+h^-)h'^{\pm}$ decays. The measurement is made with the full LHCb data set collected during Run 1 and 2 of the LHC, corresponding to an integrated luminosity of about $9\,\text{fb}^{-1}$. The analysis is under review for publication in the Journal of High Energy Physics at the time of writing [**?**] (one can hope).

4.1 Candidate reconstruction and selection

The $B^{\pm} \to D(\to K^0_S h^+h^-)h'^{\pm}$ candidates are constructed during the offline *stripping* stage described in Section 2.3.3. The candidates are defined by first combining tracks to form a $K^0_S \to \pi^+\pi^-$ vertex, then a $D \to K^0_S h^+h^-$ vertex, and finally the $B^{\pm} \to Dh'^{\pm}$ candidate. Each final state track is required to satisfy certain momentum thresholds and track-quality requirements, and to be separated from all primary interaction vertices. Each decay vertex is required to satisfy a fit-quality threshold and to be separated from the primary vertex. Momentum thresholds are applied to the composite particles and they are required to have reconstructed invariant masses close to their known masses,[1] except that the B candidate is required to have a reconstructed invariant mass in the interval 4750–7000 MeV/c^2.

[1]The exact mass window depends on the particle type and reconstruction category; narrower mass windows are applied at a later stage, as described below.

The B candidate is required to satisfy $\chi^2_{\rm IP} < 25$, where $\chi^2_{\rm IP}$ is the difference in χ^2 value of the primary vertex, when formed with- and without the B candidate. Finally, a multivariate algorithm is applied to the formed B candidate to reduce the amount of random track combinations [], denoted combinatorial background, even further than the aforementioned requirements.

Two data categories are defined, depending the tracks used to form the $K^0_{\rm S}$ candidate: the LL category where both pions are long tracks, and DD category where both pions are downstream tracks, using the track classifications of Section **??**.

Each candidate is re-analysed with the `DecayTreeFitter` (DTF) frame work [**?**], where a simultaneous fit of the full decay chain is made with a number of constraints applied: the momenta of the composite D and $K^0_{\rm S}$ particles are required to form invariant masses exactly equal to the known particle masses [**?**], and the B candidate is required to originate exactly at the primary vertex. This refit results in improved resolution of the invariant masses of the composite particles and, very importantly, of the Dalitz coordinates in the D-decay phase space, and ensures that all candidates fall in the kinematically allowed region of phase space. Unless otherwise specified, all results in this chapter are based on the refitted track momenta; for reasons explained below, some studies have to be based on parameters that are obtained without the constraints described above, or with only a subset of them applied.

Following the stripping stage, the further selection of signal candidates is performed in three steps: an initial set of requirements that remove a large fraction of candidates that are very likely to be background and veto a number of specific backgrounds, the application of a multivariate analysis algorithm designed to allow for filtering combinatorial background, and a set of particle-identification requirements are imposed. The requirements are summarised in Table **??**, and each step is described in detail in the following sections.

4.1.1 Initial requirements

At the hardware trigger level, it is required that a particle associated with the signal decay triggered the hadronic level-0 trigger (Trigger on Signal, or TOS), or that the level-0 trigger decision was caused by a particle that is not associated with the signal decay (Trigger Independent of Signal, or TIS). The inclusion of the latter category increases the data sample with X %. At the software trigger level,

Before any processing of the data, a loose preselection is applied to remove obvious background candidates. The reconstructed D ($K^0_{\rm S}$) mass is required to be within 25 (15) MeV/c^2 of the known values [**?**]. The *companion* particle, the pion or kaon produced in the $B^{\pm} \to Dh^{\pm}$ decay, is required to have associated

RICH information and a momentum less that 100 GeV/c; this ensures good particle-identification performance. Finally, all of the DTF fits of the full decay chain are required to have converged properly.

Two additional requirements are made at this stage, to suppress specific backgrounds. In order to suppress decays of the type $B^{\pm} \to K^0_S h^+ h^- h'^{\pm}$ with no intermediate D meson, so called *charmless* decays, it is required that the significance of the z-separation of the D^0 decay vertex and the $B^{\pm}$ decay vertex is above 0.5. The significance of the z-separation of the D^0 decay vertex and the $B^{\pm}$ decay vertex is defined as

$$\Delta z^{D-B}_{\text{significance}} = \frac{z^D_{vtx} - z^B_{vtx}}{\sqrt{\sigma^2(z^D_{vtx}) + \sigma^2(z^B_{vtx})}} \tag{4.1}$$

This source of background described further in section 4.2.1. In order to suppress a background from $D \to 4\pi$ and $D \to \pi\pi KK$ decays, it is required that the K^0_S flight distance χ^2_{FD} is greater than 49, where

$$\chi^2_{\text{FD}} = \left(\frac{\Delta r}{\sigma(\Delta r)}\right)^2, \tag{4.2}$$

and Δr is the measured flight distance of the K^0_S meson. This background is described in further detail in section 4.2.2. A number of the particle-identification requirements presented in Section **??** below are also introduced to reject specific background contributions.

4.1.2 Boosted decision tree

A Gradient Boosted Decision Tree [] (abbreviated BDT in the following) is applied to classify each candidate on a scale from -1 to $+1$ as signal-like ($+1$) or combinatorial-background-like (-1), based on the values of a number of input parameters for candidate in question. The BDT is implemented in the `TMVA` frame work, shipped as part of the `ROOT` data analysis package.

A boosted decision tree classifier consists of a number of sequentially trained decision trees, each of which classify events as either signal or background. Each tree bases the decision on an individual subset of variables, out of an overall set of input variables. At each training step, the input events are weighted when training a new tree, so that events that the already-trained trees classify incorrectly are given a higher weight; this is denoted boosting. The term *gradient boosting* denotes a specific weiht calculation scheme []. The final score is the average over all decision trees.

The full set of input variables are given in Table **??**. It includes the momenta of particles in the decay; a number of geometric parameters such a absolute and relative vertex positions, and distances of closest approach between tracks; $\chi^2_{\rm IP}$ values for a number of particles in the decay chain; the χ^2 per degree of freedom of the DTF refit; `DIRA` values, which denote the angle between the fitted particle momenta, and the vector spanned by it's production ad decay vertices; and finally an isolation variable, defined as

$$A_{p_T} = \frac{p_T(B) - \sum p_T(other)}{p_T(B) + \sum p_T(other)} \tag{4.3}$$

where the sum is over all other tracks in a cone around the B-candidate. The cone is defined as being within a circle with a radius of 1.5 units around the B candidate in the (η, ϕ_{azim})-plane. This variable is highly efficient in rejecting combinatorial background. Two algorithms are trained, one for the LL category of $K^0_{\rm S}$ mesons and one for the DD category, because some input parameters relate to the $K^0_{\rm S}$ meson and have very different distributions between the two categories.

The BDTs are trained and tested with input samples representing typical signal and background decay candidates: a signal sample that consists of simulated $B^{\pm} \to D(\to K^0_{\rm S}\pi^+\pi^-)\pi^{\pm}$ decays corresponding to the LHCb running conditions for the years 2012–2018, and a sample of combinatorial background candidates from real data, where the reconstructed invariant mass of the B meson is larger than $5800\,{\rm MeV}/c^2$. The candidates in both samples were required to have passed the initial requirements described in the preceding section. The distributions of the input parameters in the signal and background training samples are shown in Figs. **??** and **??**. The signal and background samples are each split into two before the training stage: one sub sample, the training sample, is used to train the BDT, after which it is applied to the other sub sample, the test sample. The classifier is found to perform well on the test sample, not just the training sample, which ensures that it does not suffer significant overtraining. The BDT output distribution are shown for both test and training samples in Fig. **??**, where it is clear that the classifier very effectively separates signal and background candidates.

Each candidate in data is classified using the BDT, and candidates that are assigned a score below some threshold value are discarded. The threshold values are chosen in a set of pseudo experiments, such that the expected sensitivity to γ is maximised. This is done by performing preliminary fits to the data set for a range of different BDT threshold values, then generating many pseudo data sets with the obtained yields, and applying the full fit and interpretation

procedure described in Section **??** and **??** to each data set. The procedure is applied independently for the LL and DD categories, as well as for the Run 1 and Run 2 data sets, because some parameter distributions differ slightly between the two runs. The optimal threshold values are found to be 0.8 in all situations, except for LL candidates in Run 1 where it is 0.6. This is illustrated in Fig. **??** where the results of the threshold scans are shown. While the classifiers were trained using samples of $B^\pm \to D(\to K^0_S\pi^+\pi^-)\pi^\pm$ simulation and data, they are applied to the $B^\pm \to DK^\pm$ and $D \to K^0_S K^+ K^-$ samples as well; the decays are similar enough that no significant improvement in performance was obtained when considering a more elaborate setup. Across all categories, the requirement on the BDT output is found to remove approximately 98 % of the combinatorial background, while being approximately 93 % efficient on signal.

4.1.3 Particle-identification requirements

PID cuts are used to separate $B^\pm \to DK^\pm$ and $B^\pm \to D\pi^\pm$ candidates in the samples used in this analysis:

- For the $B^\pm \to D(\to D \to K^0_S h^+ h^-)\pi^\pm$ samples we require that PIDK < 4 for the bachelor.
- For the $B^\pm \to D(\to D \to K^0_S h^+ h^-)K^\pm$ samples we require that PIDK > 4 for the bachelor.

Furthermore, PID requirements are made to suppress semi-leptonic backgrounds and decays where a final state particle decays in flight, and a a loose PID requirement is made in the $D \to K^0_S K^+ K^-$ channels to suppress background contributions:

- the companion particle is required to satisfy `IsMuon` $= 0$.
- For the $B \to D(\to K^0_S\pi^+\pi^-)h^\pm$ samples it is require that the charged pion track from the D decay with opposite charge to the companion satisfies PIDe < 0 & `IsMuon` $= 0$, and for the other charged pion that `IsMuon` $= 0$.
- For the $B \to D(\to K^0_S K^+ K^-)h^\pm$ samples it is required that the charged kaon tracks from the D decay have RICH information, a momentum less than 100 GeV/c and PIDK > -5 & `IsMuon` $= 0$.

These backgrounds and requirements are described in Section 4.2.3.

4.1.4 Final requirements

For a small sample of candidates in the final sample, it is the case that one or more candidates originate in the same pp collision. In order to make sure that all candidates are completely independent, only one candidate from each pp collision is kept in this case, and the others discarded. The choice of candidate to keep in arbitrary. This requirements results in the removal of less than 0.7 % of candidates in each data category.

Furthermore, the D mass used to define the binning schemes described in Ref. [**?**] differs slightly from the mass used in the DTF refit. Therefore a few of the decays are reconstructed with Dalitz coordinates outside the allowed kinematic region. Because this problem only concerns a handful of candidates, they are simply discarded.

4.1.5 Selected candidates

In total, about X $B^{\pm} \to DK^{\pm}$ candidates and Y $B^{\pm} \to D\pi^{\pm}$ candidates are selected, as summarised in Table **??**. The B mass distribution in the various data categories are shown in Figs. **??** and **??** at various stages of the selection, and the Dalitz plots for candidates in the signal region where $m_B \in [5249, 5309]\,\mathrm{MeV}/c^2$ are shown in Fig. **??** and **??**. Given the large yields in the full Run 1 and 2 LHCb data set, the asymmetries between the B^+ and B^- distributions are visible in the $B^{\pm} \to DK^{\pm}$ plots.

4.2 Background studies

A wide range of backgrounds can potentially pollute the sample of signal candidates. The backgrounds naturally group into three categories depending on how they are treated in the analysis:

- Backgrounds that can be effectively removed in the selection
- Backgrounds that are only present at a level where the impact on the measurement result is small, and which do therefore not have to be modelled
- Backgrounds that are present at a level where they have to be modelled in the fit to data, and cannot effectively be rejected further in the selection

The latter category comprises of combinatorial background, which remains present at a non-negligible level after the application of the BDT described in Section **??**; contributions from a number of partly reconstructed $B \to Dh^{\pm}X$ decays, where

X denotes a pion or photon that is not included in the reconstructed decay, and which can only be separated from signal decays by their $m(Dh)$ distribution; and finally $B^\pm \to D\pi^\pm$ decays that are categorised as $B^\pm \to DK^\pm$ decays in the particle-identification step and vice-versa. These background sources are described in detail in Section **??**. This section focuses on backgrounds that led to specific requirements in the selection or proved to be small enough not to merit special treatment.

4.2.1 Charmless decays

4.2.2 Background from four-body D decays

4.2.3 Semi-leptonic backgrounds

Discuss particles that decay in flight as well

4.2.4 Cross-feed from other $D \to K^0_S h^+ h'^-$ decays

4.2.5 Swapped-track backgrounds

4.3 Signal and background mass shapes

The measurement employs *extended maximum-likelihood fits* to the $m(Dh^\pm)$ distribution of signal candidates to determine the observables of interest. The analysis implements a two-step fit procedure: first the data samples are analysed without separating the candidates by B charge or Dalitz bin, in order to determine appropriate parametrisations of the $m(Dh^\pm)$ distribution of the signal and relevant background components. These parameterisations are then kept fixed in a subsequent fit that obtains the observables of interest by parameterising the signal yield in each Dalitz bin via the equations derived in Chapter 1. This section describes the first step, whereas the latter fit is the subject of Section 4.4.

The candidates are split in 8 categories depending on whether the bachelor is categorised as a kaon or pion, whether the K^0_S meson is in the LL or DD category, and by whether the D meson is reconstructed in the $K^0_S\pi^+\pi^-$ or $K^0_S K^+ K^-$ final state (in the second fit they are further split by charge and Dalitz bin). For each category c the likelihood function is defined

$$\mathcal{L}_c \equiv N^{sig,c} f_s(\theta_s) + \sum_i N_i^{bkg,c} f_i(\theta_i) \tag{4.4}$$

4.4 Measurement of the CP-violation observables

4.5 Systematic uncertainties

4.6 Obtained constraints on γ